CDDpress

www.nature.com/cdd

ARTICLE

Check for updates

BAP1 promotes the repair of UV-induced DNA damage via PARP1-mediated recruitment to damage sites and control of activity and stability

Shin-Ai Lee[1,7,8], Daye Lee[1,8], Minhwa Kang[1,8], Sora Kim[1,8], Su-Jung Kwon[1], Han-Sae Lee[1], Hye-Ran Seo[1], Prashant Kaushal[2,3], Nam Soo Lee[4], Hongtae Kim[5], Cheolju Lee[2,6] and Jongbum Kwon[1]✉

BRCA1-associated protein-1 (BAP1) is a ubiquitin C-terminal hydrolase domain-containing deubiquitinase with tumor suppressor activity. The gene encoding BAP1 is mutated in various human cancers, with particularly high frequency in kidney and skin cancers, and BAP1 is involved in many cancer-related cellular functions, such as DNA repair and genome stability. Although BAP1 stimulates DNA double-strand break repair, whether it functions in nucleotide excision repair (NER) is unknown. Here, we show that BAP1 promotes the repair of ultraviolet (UV)-induced DNA damage via its deubiquitination activity in various cell types, including primary melanocytes. Poly(ADP-ribose) polymerase 1 (PARP1) interacts with and recruits BAP1 to damage sites, with BAP1 recruitment peaking after the DDB2 and XPC damage sensors. BAP1 recruitment also requires histone H2A monoubiquitinated at Lys119, which accumulates at damage sites. PARP1 transiently poly(ADP-ribosyl)ates (PARylates) BAP1 at multiple sites after UV damage and stimulates the deubiquitination activity of BAP1 both intrinsically and via PARylation. PARP1 also promotes BAP1 stability via crosstalk between PARylation and ubiquitination. Many PARylation sites in BAP1 are mutated in various human cancers, among which the glutamic acid (Glu) residue at position 31, with particularly frequent mutation in kidney cancer, plays a critical role in BAP1 stabilization and promotes UV-induced DNA damage repair. Glu31 also participates in reducing the viability of kidney cancer cells. This study therefore reveals that BAP1 functions in the NER pathway and that PARP1 plays a role as a novel factor that regulates BAP1 enzymatic activity, protein stability, and recruitment to damage sites. This activity of BAP1 in NER, along with its cancer cell viability-reducing activity, may account for its tumor suppressor function.

Cell Death & Differentiation (2022) 29:2381–2398; https://doi.org/10.1038/s41418-022-01024-w

INTRODUCTION

The mammalian nucleotide excision repair (NER) pathway repairs structurally unrelated bulky DNA lesions, including ultraviolet (UV) radiation-induced cyclobutane-pyrimidine dimers (CPDs). Global genome NER (GG-NER) is a dominant subpathway of NER that detects and eliminates bulky damages in the entire genome. The repair process involves a series of steps for damage recognition, removal of the damaged DNA by a double incision, synthesis of new stretches of nucleotides and, finally, DNA ligation. DNA damage-binding protein 1 (DDB1)/DDB2 complex and xeroderma pigmentosum group C-complementing protein (XPC) play crucial role in recognizing damages during GG-NER [1–3].

Poly(ADP-ribose) polymerase 1 (PARP1), the dominant and founding member of PARP family, chemically attaches ADP-ribose groups to target proteins by using nicotinamide adenine dinucleotide (NAD^+) as an ADP-ribose donor, resulting in the formation of negatively charged linear or branched polymeric chains termed poly(ADP-ribose) (PAR) chains on the target proteins [4, 5]. PARP1 plays important role in NER and other types of DNA repair, such as double-strand break (DSB) repair. Upon induction of DNA damage, PARP1 rapidly localizes at damage sites through its DNA binding ability, leading to PARylation of itself (auto-PARylation) and of multiple other targets, which promotes recruitment of repair proteins to damage sites [3, 6, 7]. PARP1 has been documented to play role in recruitment of DDB1/2 and XPC to damage sites to stimulate DNA repair during GG-NER [8–11].

BRCA1-associated protein-1 (BAP1) is a ubiquitin C-terminal hydrolase (UCH) domain-containing deubiquitinase (DUB) with tumor suppressor activity [12–15]. Inactivating mutations in *BAP1* are found in diverse human cancers, including mesothelioma, uveal melanoma, cutaneous melanoma, and renal cell carcinoma (RCC) [16–21]. All carriers of inherited heterozygous *BAP1*-

[1]Department of Life Science, The Research Center for Cellular Homeostasis, Ewha Womans University, 52 Ewhayeodae-gil, Seodaemun-gu, Seoul 03760, Korea. [2]Center for Theragnosis, Korea Institute of Science and Technology, Seoul 02792, Korea. [3]Division of Bio-Medical Science & Technology, KIST School, Korea University of Science and Technology, Seoul 02792, Korea. [4]Department of Biological Sciences, Sungkyunkwan University, Suwon 16419, Korea. [5]School of Life Sciences, Ulsan National Institute of Science and Technology, Ulsan 44919, Korea. [6]KHU-KIST Department of Converging Science and Technology, Kyung Hee University, 26 Kyunghee-daero, Dongdaemun-gu, Seoul 02447, Korea. [7]Present address: Laboratory of Genitourinary Cancer Pathogenesis, Center for Cancer Research, National Cancer Institute, Building 37, Room 1068, Bethesda, MD 20892-4263, USA. [8]These authors contributed equally: Shin-Ai Lee, Daye Lee, Minhwa Kang, Sora Kim. ✉email: jongkwon@ewha.ac.kr

Edited by K. Newton

Received: 13 October 2021 Revised: 18 May 2022 Accepted: 19 May 2022
Published online: 30 May 2022

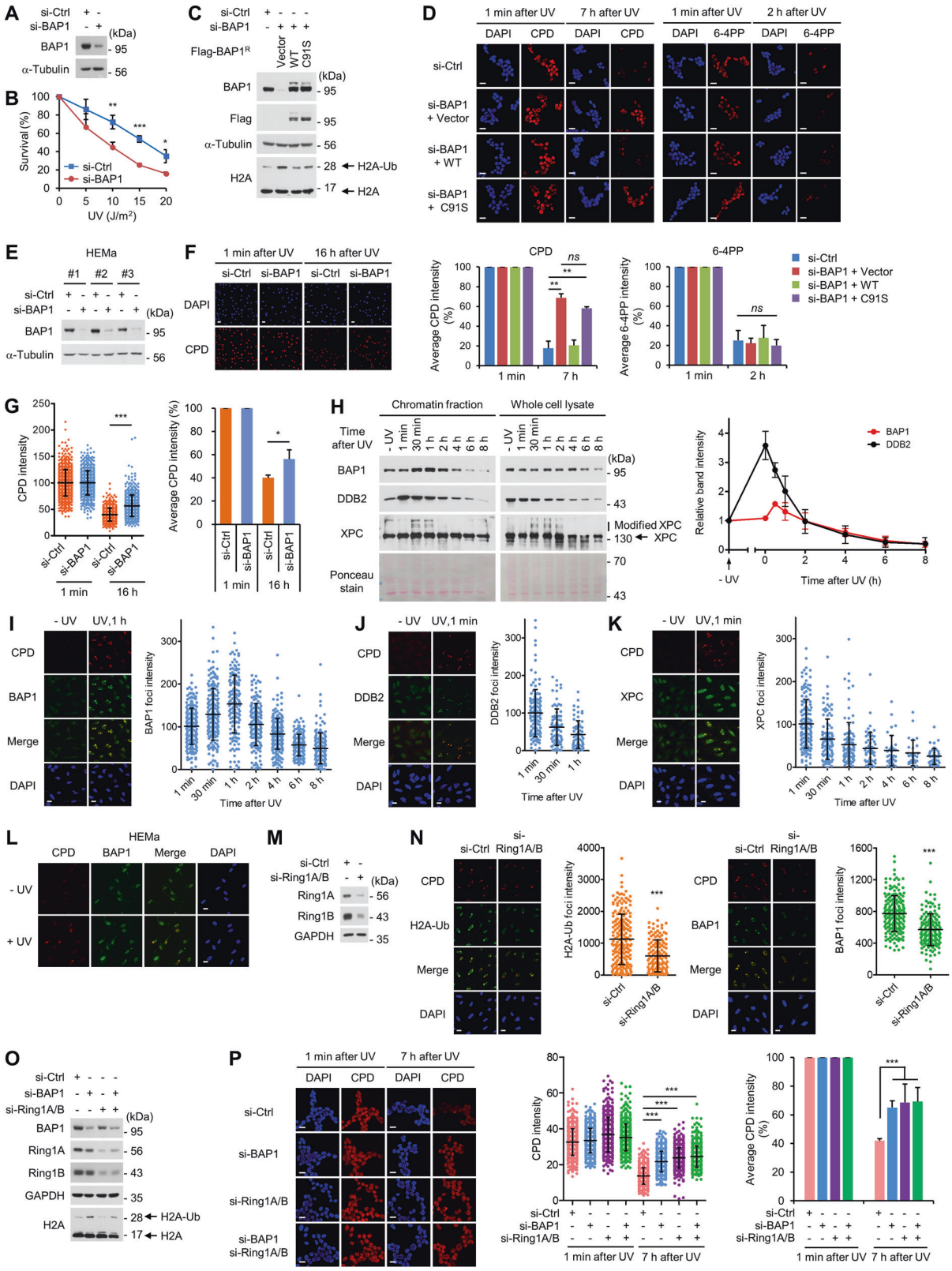

inactivating mutations develop at least one and often multiple cancers during their lifetimes (called BAP1 cancer syndrome), and acquired biallelic *BAP1* mutations are common in human cancers [13, 21, 22]. Gene targeting studies with mice support tumor suppressor function of BAP1 [23–26]. Consistent with its tumor suppressor activity, BAP1 has functions in many cancer-associated cellular processes, such as cell cycle control [27–29], cell death [30], the DNA damage response (DDR) [31, 32], DNA replication [33–35], and genome stability [15, 31, 34, 36]. Studies have shown that BAP1 is recruited to DSBs and promotes DNA repair [31, 37]. However, whether BAP1 functions in other types of DNA repair, such as NER, remains unknown.

Fig. 1 BAP1 is recruited to UV damage sites and promotes DNA repair. A siRNA knockdown of BAP1 in 293T cells. **B** Colony formation assay showing that 293T cells become hypersensitive to UV irradiation upon BAP1 knockdown. $n = 3$; error bars, mean ± s.d. **C** Immunoblots showing the expression of siRNA-resistant (^{R}) versions of wild-type or C91S-mutant Flag-BAP1 in BAP1-depleted 293T cells. H2A-Ub was analyzed as a means to monitor BAP1 activity. **D** BAP1 knockdown reduces CPD repair in 293T cells. After transfection as described in **C**, cells were irradiated with UV light (25 J/m^2) and fixed immediately (1 min) or after 7 h (for CPD) or 2 h of recovery (for 6-4PP) for immunofluorescence microscopy. Representative confocal images (top) and the graph of the average CPD and 6-4PP intensities are shown (bottom). $n = 3$; error bars, mean ± s.d. Scale bar, 10 μm. **E** siRNA knockdown of BAP1 in HEMa cells (three independent experiments). **F** Representative results showing the effects of BAP1 knockdown on CPD repair after UV irradiation (10 J/m^2) in HEMa cells. Scale bar, 20 μm. **G** (Left) The CPD staining intensity values under each experimental condition as described in **F** were pooled from three independent experiments and shown as a scatter plot. Cell counts: 890, 845, 811, and 817 (in the same order as presented in the graph). (Right) Percentages of the average CPD staining intensity per experimental condition are shown as a bar graph. $n = 3$; error bars, mean ± s.d. **H** (Left) U2OS cells were irradiated with UV light (25 J/m^2) and harvested at various time points, and the chromatin binding of BAP1, DDB2 and XPC was analyzed by cell fractionation. A representative result is shown. (Right) The intensities of the indicated protein bands were quantitated by densitometry and depicted graphically by setting the value for the first lane of each protein to 1. $n = 3$; error bars, mean ± s.d. The response of XPC to UV irradiation was qualitatively evaluated by the production of the modified protein. **I**–**K** Results of the micropore assay. U2OS cells were exposed to UV irradiation (25 J/m^2) through a micropore filter and fixed at various time points for immunostaining for CPD along with BAP1 (**I**, cell counts: 158–246), DDB2 (**J**, cell counts: 67–130) or XPC (**K**, cell counts: 29–153). The data are shown as a scatter plot on the right. The lines indicate the mean ± s.d. values. Representative confocal images are shown for one time point only and the images for all time points are shown in Supplementary Fig. 1D–F. Scale bar, 20 μm. **L** Results of a micropore assay similar to that described in (**I**) showing BAP1 foci formation in irradiated HEMa cells. Cells were fixed immediately after UV irradiation (25 J/m^2). Scale bar, 20 μm. **M** Knockdown of Ring1A/B in U2OS cells by cotransfection with siRNAs specific for Ring1A or Ring1B. **N** Results of a micropore assay with the cells in **M**, showing the effects of Ring1A/B knockdown on the formation of H2A-Ub (cell counts: 138–197) and BAP1 foci (cell counts: 154–193) 4 h and 1 h after UV irradiation (25 J/m^2), respectively. Scale bar, 20 μm. **O** siRNA knockdown of BAP1, Ring1A/B, or both in 293T cells. H2A-Ub was also analyzed to monitor the knockdown effects. **P** Results of a CPD repair assay with the cells in **O**. The data were processed as in **G**. Cell counts for the scatter plot: 591, 560, 459, 551, 518, 526, 545, and 511 (in the same order as presented in the graph). $n = 3$; error bars, mean ± s.d.

In this study, we showed that BAP1 promotes the repair of UV-induced DNA damage via its DUB activity and that PARP1 interacts with and recruits BAP1 to damage sites and stimulates BAP1 activity intrinsically and via PARylation. We also showed that many PARylation sites in BAP1 are mutated in multiple human cancers, and one site is involved in BAP1 stability and DNA repair activity as well as in cancer cell viability.

RESULTS

BAP1 promotes the repair of UV-induced DNA damage

We set out to investigate whether BAP1 functions in the repair of UV-induced DNA damage. BAP1 depletion rendered 293T cells hypersensitive to UV-C light (254 nm, hereafter denoted UV) (Fig. 1A, B), and greatly compromised the repair of CPD with little effect on the repair of 6-4PP (Fig. 1C, D). Notably, complementation by BAP1 but not the C91S catalytic mutant rescued the defect in CPD repair in BAP1-depleted cells (Fig. 1C, D). BAP1 depletion reduced CPD repair in primary melanocytes (Fig. 1E–G and Supplementary Fig. 1A) and clear cell renal cell carcinoma (ccRCC) cells (see Fig. 8 below). BAP1 bound chromatin after UV irradiation (Supplementary Fig. 1B), which increased transiently peaking at 30 and 60 min (Fig. 1H and Supplementary Fig. 1C). The UV-induced chromatin binding of BAP1 was modest and slower than that of DDB2, which exhibited a robust and rapid response to UV irradiation, as reported (Fig. 1H) [10]. Posttranslational modifications of XPC were detected in the chromatin fractions after UV irradiation, as previously shown [8] (Fig. 1H). BAP1 formed clear foci overlapping with CPD immediately after UV irradiation in U2OS cells; the intensity of the foci peaked at 30 and 60 min, remaining significant until the CPD signals disappeared (Fig. 1I and Supplementary Fig. 1D). In contrast, DDB2 and XPC foci formed only immediately after UV irradiation (Fig. 1J, K and Supplementary Fig. 1E, F). BAP1 foci overlapping CPD were also detected in UV-irradiated primary melanocytes (Fig. 1L). BAP1 depletion did not significantly affect the chromatin binding of DDB2 and modified XPC (Supplementary Fig. 1G) or the formation of DDB2 and XPC foci after UV irradiation (Supplementary Fig. 1H–J). These results collectively suggest that BAP1 directly promotes CPD repair via its DUB activity, which is cell type-independent, probably by participating in the entire repair process, but is unlikely to function in damage recognition.

Histone H2A monoubiquitinated at Lys119 (H2A-Ub-K119, hereafter denoted H2A-Ub) functions in NER[1]. H2A-Ub formed clear foci overlapping with CPD immediately after UV irradiation, peaking at 4 h (Supplementary Fig. 1K). Depletion of Ring1A and Ring1B, the major E3 ligases for H2A, greatly reduced both H2A-Ub foci and BAP1 foci (Fig. 1M, N). Ring1A/B depletion reduced CPD repair to the similar extent as BAP1 depletion and this repair defect was not further exacerbated by depletion of both Ring1A/B and BAP1 (Fig. 1O, P). These results suggest that H2A-Ub promotes CPD repair via BAP1 recruitment to damage sites.

BAP1 interacts with PARP1 in response to UV damage

Next, we sought to identify the cellular proteins that interact with BAP1 in a UV damage-dependent manner. Immunoprecipitation (IP) from Flag-BAP1-expressing 293T cells showed that, among numerous proteins that coprecipitated with Flag-BAP1, one distinct protein band increased in intensity after UV irradiation (Fig. 2A). This UV-induced protein was identified as PARP1 by MS analysis (Fig. 2B and Supplementary Fig. 2A, B). The interaction between BAP1 and PARP1 and its induction by UV irradiation were confirmed by reciprocal co-IP for the epitope-tagged (Fig. 2C, D) and endogenous proteins (Fig. 2E, F). The interaction between BAP1 and PARP1 was direct, as assessed by in vitro pulldown assays (Fig. 2G). Protein mapping with a set of deletion mutants showed that the DBD is critical for PARP1 to interact with BAP1 (Fig. 2H, I). While the HBM-containing central region of BAP1 is important for its interaction with PARP1 (Fig. 2J, K), the mutant BAP1 lacking this region (UCH-CTD) still interacts with PARP1 and this interaction does not increase after UV irradiation (Fig. 2J, L, and Supplementary Fig. 2C, D). Therefore, it appears that BAP1 interacts with PARP1 using multiple domains and the integrity of the whole protein is important for the UV-induced interaction with PARP1.

Interestingly, the interaction between BAP1 and PARP1 increased after treatment with ionizing radiation, etoposide and hydroxyurea (Supplementary Fig. 2E, F), which may be functionally meaningful in DSB repair and replication stress recovery. BAP1 phosphorylation at Ser592, important for the repair of DSBs and UV damage [31, 32, 37], is not important for its interaction with PARP1 since removal of phosphate groups from BAP1 by phosphatases (Supplementary Fig. 2G) or mutation of Ser592 to a nonphosphorylatable or phosphomimetic amino

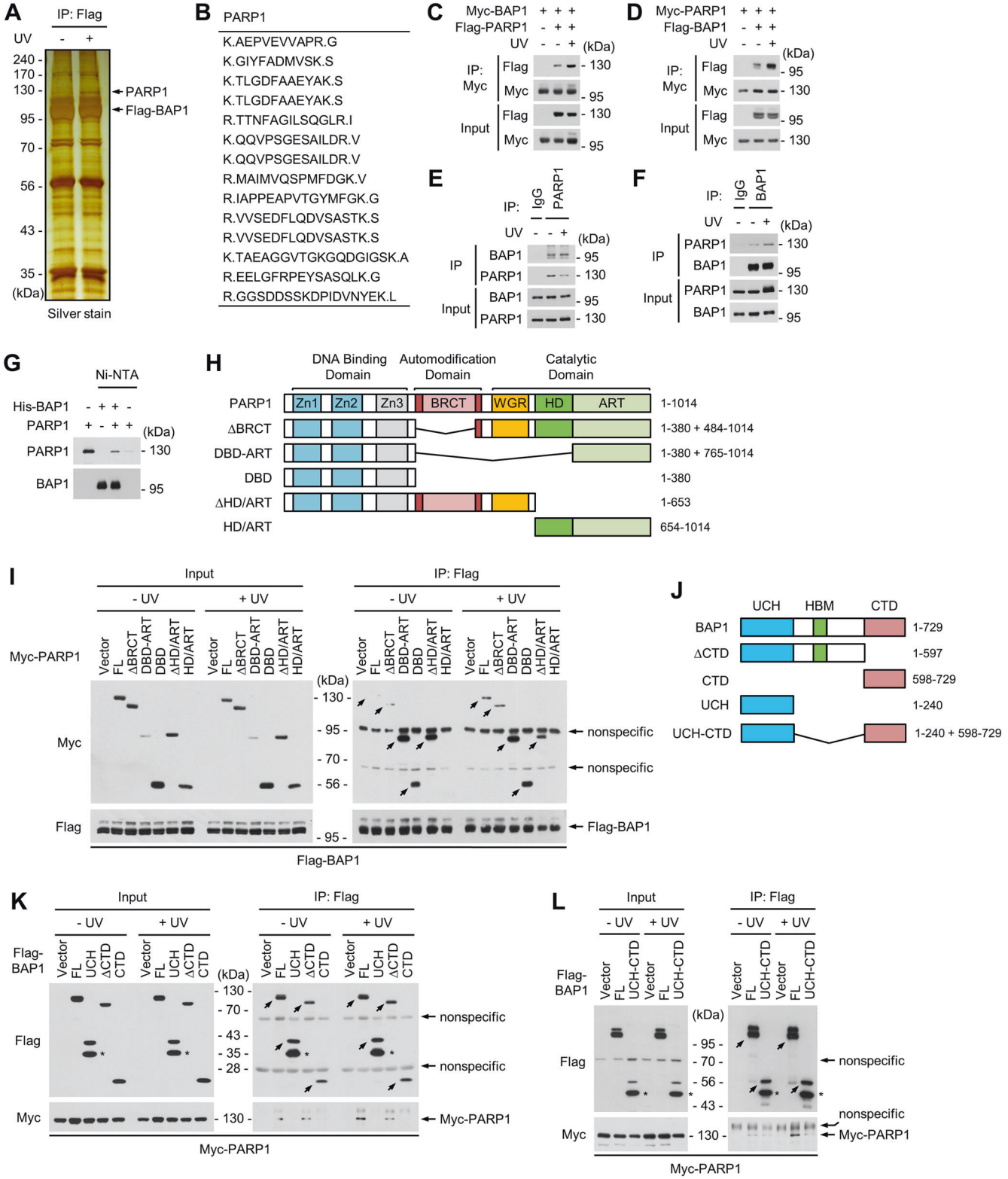

acid residue (Supplementary Fig. 2H) had no effect on its interaction with PARP1.

PARP1 PARylates BAP1 in response to UV damage

To determine whether PARP1 PARylates BAP1, we performed an in vivo PARylation assay. PARylation of Flag-BAP1, manifested by a mobility shift and detection with an anti-PAR antibody, occurred in untreated cells, increasing transiently and peaking 30 min after UV irradiation (Fig. 3A) in a manner dependent on the UV dose (Fig. 3B). PARP1 depletion or treatment with PARP inhibitors (PARPis), such as E7449 and olaparib, abolished BAP1 PARylation under both untreated and UV-treated conditions (Fig. 3C, D), indicating that PARP1 is responsible for BAP1 PARylation. Flag-BAP1 and Myc-PARP1 (Flag-PARP1 also) immunoprecipitates did

Fig. 2 BAP1 interacts with PARP1 in response to UV damage. A Silver-stained gel of the immunoprecipitated samples from untreated and UV-treated 293T cells expressing Flag-BAP1 (1 h after 50 J/m^2 irradiation). The protein bands marked as PARP1 were excised and subjected to MS analysis. **B** Sequences of the peptides matching PARP1 in MS analysis. Results of reciprocal co-IP for the interaction between BAP1 and PARP1 before and after UV treatment (50 J/m^2) in 293T cells expressing Myc-BAP1 and Flag-PARP1 (**C**) and in cells expressing Flag-BAP1 and Myc-PARP1 (**D**). **E**, **F** Results of reciprocal co-IP for the interaction between endogenous BAP1 and PARP1 before and after UV treatment (1 h after 50 J/m^2 irradiation). **G** In vitro pulldown assay using purified recombinant His-BAP1 and PARP1. **H** Schematic diagram of Myc-PARP1 mutants lacking protein domains in various combinations. PARP1 has three main functional domains: the N-terminal DNA binding domain (DBD) comprising three zinc fingers, the central automodification domain containing a BRCA1 C-terminal (BRCT) motif, and the C-terminal catalytic domain consisting of the tryptophan-glycine-arginine (WGR) domain, a helical domain (HD) and the ADP-ribosyltransferase (ART) domain. **I** Mapping results from co-IP for the interactions between Flag-BAP1 and Myc-PARP1 deletion mutants in untreated and UV-treated 293T cells (1 h after 50 J/m^2 irradiation). A representative of four independent experiments with similar results is shown. The coprecipitated full-length (FL) and mutant Myc-PARP1 proteins are indicated by tilted arrows. **J** Schematic diagram of the Flag-BAP1 deletion mutants. UCH ubiquitin C-terminal hydrolase domain, HBM HCF-1 binding motif, CTD C-terminal domain. **K**, **L** Mapping results from co-IP for the interactions between Flag-BAP1 deletion mutants and Myc-PARP1 in untreated and UV-treated 293T cells (1 h after 50 J/m^2 irradiation). A representative of three (**K**) and two independent experiments (**L**) with similar results is shown. The precipitated FL and mutant Flag-BAP1 proteins are indicated by tilted arrows. The star indicates a degraded form of UCH (**K**) and UCH-CTD (**L**).

not contain PARP1 and BAP1, respectively (Fig. 3E), excluding the possibility that the PAR signals in the Flag-BAP1 immunoprecipitates were produced by associated auto-PARylated PARP1. We confirmed PARylation of endogenous BAP1 and its increase after UV damage by reciprocal co-IP (Fig. 3F, G). Interestingly, the interaction between BAP1 and PARP1 transiently increased after UV irradiation, peaking at 30 min and 6 h (Fig. 3H and Supplementary Fig. 3B), however, BAP1 PARylation peaked only at 30 min (Fig. 3I). PARPi treatment did not affect the interaction between BAP1 and PARP1 (Fig. 3J). Therefore, the interaction between BAP1 and PARP1 is independent of PARylation and does not necessarily lead to BAP1 PARylation.

Contrary to our expectations that PARP1 overexpression would increase BAP1 PARylation, ectopic expression of Myc-PARP1 instead decreased BAP1 PARylation regardless of UV exposure (Supplementary Fig. 3A). Increasing expression of Myc-PARP1 resulted in a dose-dependent decrease in total protein PARylation, including that of BAP1 (Supplementary Fig. 3C). Excessive PARP1 might have disrupted the cellular homeostasis of protein PARylation activity.

PARP1 recruits BAP1 to UV damage sites to stimulate DNA repair

Given that PARP1 recruits many DDR proteins to UV damage sites[3], we investigated whether it also functions in BAP1 recruitment. Both PARP1 depletion (Fig. 4A, B and Supplementary Fig. 4A) and PARPi treatment reduced BAP1 chromatin binding and BAP1 colocalization with CPDs after UV irradiation (Fig. 4C, D and Supplementary Fig. 4B, C). Similar effects of PARP1 depletion and PARPi treatment were observed for transfected GFP-BAP1 (Supplementary Fig. 4D, E). These results suggest that PARP1 recruits BAP1 to UV damage sites and that PARP1 activity is important for this process. GFP-PARP1 accumulated at damage sites faster than GFP-BAP1, as shown by live-cell microscopy combined with laser microirradiation (UV-A, 405 nm) (Supplementary Fig. 4F, G), consistent with the report that BAP1 accumulation at sites of laser-induced DNA damage is dependent on PARP1 [37]. Although the laser generates DNA breaks in addition to CPDs and the recruitment kinetics may thus differ [38], these results support the role of PARP1 in BAP1 recruitment to UV damage sites.

ATM kinase is recruited to damage sites for NER [39, 40]. ATM inhibitor (ATMi) treatment reduced BAP1 chromatin binding (Fig. 4C and Supplementary Fig. 4B) and BAP1 colocalization with CPDs after UV irradiation (Fig. 4D and Supplementary Fig. 4C). Simultaneous treatment with a PARPi and an ATMi did not produce a combined effect on BAP1 recruitment to damage sites (Fig. 4D). While a PARPi or ATMi alone inhibited CPD repair, combination treatment did not enhance the inhibitory effects of the individual drugs (Fig. 4E). Thus, it appears that ATM plays a role in BAP1-mediated CPD repair, likely via the same pathway as PARP1.

Although BAP1 depletion and PARP1 depletion impaired CPD repair to similar degrees, combined depletion of BAP1 and PARP1 did not reduce CPD repair beyond the levels achieved by depletion of either alone (Fig. 4F, G). Importantly, the UCH-CTD-mutant BAP1, which lacks a UV-induced PARP1 binding activity, did not rescue the defect in CPD repair in BAP1-depleted cells (Fig. 4H, I). These results, in keeping with the activity of PARP1 in recruiting BAP1 to damage sites, suggest that BAP1 functions in CPD repair as a major target of PARP1.

PARP1 PARylates BAP1 at multiple sites in vitro

To characterize BAP1 PARylation in depth, we performed an in vitro PARylation assay using purified recombinant proteins (Supplementary Fig. 5A). As expected, PARP1 alone underwent auto-PARylation dependent of NAD^+ (Fig. 5A, lanes 1 and 2). Notably, coincubation of PARP1 and BAP1 resulted in a mobility shift of BAP1 to a slowly migrating species, which was detected by the anti-PAR antibody, indicating that the shifted species was PARylated BAP1. BAP1 PARylation was specific as it occurred dependent of NAD^+ and activated DNA (Fig. 5A, lanes 3 and 4; Supplementary Fig. 5B) and increased proportionally with reaction time (Fig. 5B). PARP1 PARylated BAP1-C91S as efficiently as BAP1 (Supplementary Fig. 5B). Thus, PARP1 PARylates BAP1 directly and the DUB activity of BAP1 is not necessary for its PARylation. Notably, auto-PARylated PARP1 did not readily enter the resolving gel and was barely detected on the gel after the extended PARylation reaction (Fig. 5B and Supplementary Fig. 5B, C), likely due to both its greatly increased molecular weight and possible insoluble aggregation.

To identify the PARylation sites in BAP1, we treated the BAP1 PARylation reactions (Supplementary Fig. 5D) with hydroxylamine (NH_2OH), which cleaves the ester bond between the first ADP-ribose unit of PAR and the side-chain carboxyl group of an Asp or Glu residue [41]. We then digested the proteins with trypsin and used LC-MS/MS to detect trypsinized peptides containing a hydroxamic acid derivative of Asp or Glu residues that weighed 15.0105 Da more than the corresponding unmodified peptides. We identified eight unambiguous and 29 ambiguous sites of ADP-ribosylation in BAP1, among which 24 were on Asp residues and 13 on Glu residues (Fig. 5C, D and Supplementary Fig. 5E). Most ADP-ribosylation sites (29 of 37) were located in the central region between the positions 240 and 635, whereas eight sites were located in the termini of the UCH domain (Fig. 5C).

PARP1 regulates the catalytic activity of BAP1 both intrinsically and via PARylation

To determine whether PARP1 affects BAP1, we performed an in vitro PARylation-coupled DUB assay using Ub-AMC as a

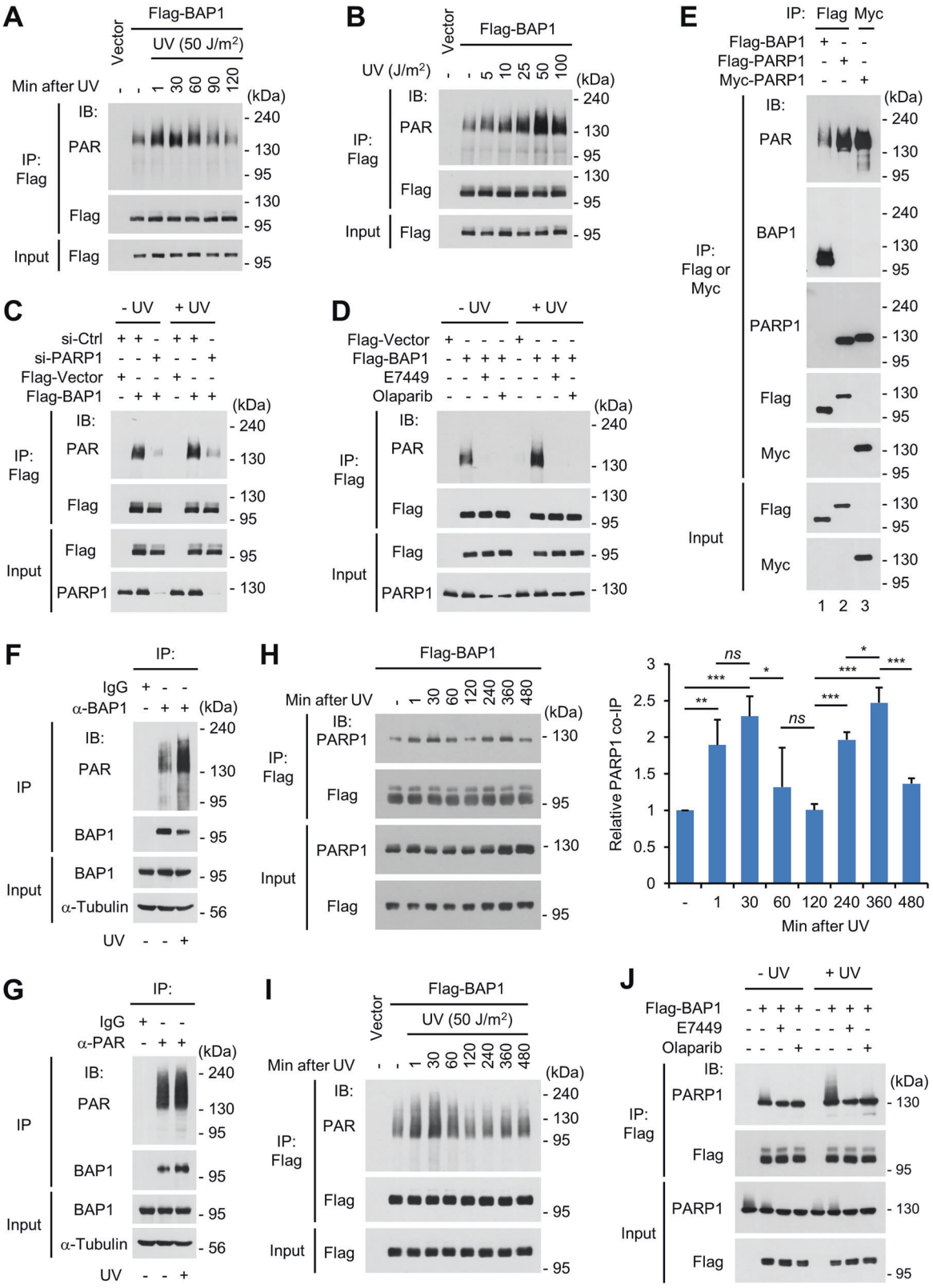

BAP1 substrate (Fig. 6A and Supplementary Fig. 6A). Incubation of BAP1 with PARP1 in the presence of NAD^+ increased its DUB activity, with this activity increasing proportionally with the PARylation reaction time (Fig. 6B, C). As control, neither BAP1-C91S nor PARP1 alone exhibited DUB activity (Fig. 6B). Interestingly, PARP1 stimulated BAP1 activity in the absence of NAD^+ (Fig. 6D), which was enhanced by PARylation (Fig. 6E). These data show that PARP1 stimulates BAP1 both intrinsically and via PARylation. Then, we examined this PARP1 activity using a more physiological substrate, H2A-Ub assembled into a nucleosome (Fig. 6F and Supplementary Fig. 6B–E). Surprisingly, PARP1-mediated PARylation almost completely abolished the BAP1

Fig. 3 PARP1 PARylates BAP1 in response to UV damage. A Results of the in vivo PARylation assay showing a transient increase in Flag-BAP1 PARylation after UV irradiation. **B** Results of the in vivo PARylation assay showing a dose-dependent increase in Flag-BAP1 PARylation (harvested 30 min after UV irradiation). **C** After cotransfection with PARP1 siRNA and the Flag-BAP1 expression vector, cells were harvested 30 min after UV irradiation (25 J/m^2) for an in vivo PARylation assay. **D** After transfection with Flag-BAP1, cells were treated with a PARPi (E7499 or olaparib, each 10 μM) 30 min before UV irradiation and harvested 60 min later for an in vivo PARylation assay. **E** Results of the in vivo PARylation assay showing that the PAR signals of Flag-BAP1 are not produced by associated auto-PARylated PARP1. **F**, **G** Results of the in vivo reciprocal PARylation assay showing that endogenous BAP1 is PARylated and that this PARylation increases after UV irradiation. BAP1 (**F**) and PARylated proteins (**G**) were immunoprecipitated with anti-BAP1 and anti-PAR antibodies, respectively, and the anti-BAP1 and anti-PAR precipitates were analyzed by immunoblotting for PARylation and BAP1, respectively. **H** After transfection with Flag-BAP1, cells were harvested at various time points up to 8 h after UV irradiation (25 J/m^2) for co-IP to evaluate the interaction between Flag-BAP1 and PARP1. The PARP1 band intensity was quantified by densitometry and depicted graphically by setting the value for the first lane to 1. $n = 3$; error bars, mean ± s.d. **I** Results of the in vivo PARylation assay showing that Flag-BAP1 PARylation had one peak at 30 min after UV irradiation during an extended time course up to 8 h. **J** Results of co-IP showing that the interaction between Flag-BAP1 and PARP1 is independent of PARylation. PARPi treatment and UV irradiation were performed as described in **D**. All experiments in this figure were performed using 293 T cells and a 25 J/m^2 dose of UV irradiation (except for those in **B**).

activity toward nucleosomal H2A-Ub (Fig. 6G, lane 5), even under conditions permitting maximal BAP1 activity (Fig. 6H, lane 3), and this inhibition increased proportionally with the BAP1 PARylation reaction time (Fig. 6I, lanes 4–9). PARylation-dependent BAP1 inhibition still occurred when PARylation was terminated by PARPi before incubation with H2A-Ub nucleosomes (Fig. 6J, lanes 4–7), excluding the possibility that potential histone PARylation restricted the access of BAP1 to nucleosomes. In similar reactions, inclusion of excess amounts of ASXL1^{DEU} did not rescue PARylation-dependent BAP1 inhibition (Fig. 6K, lane 7), indicating that ASXL1^{DEU} was not the limiting factor. Therefore, we concluded that PARylation specifically rendered BAP1 inactive toward nucleosomal H2A-Ub.

It was intriguing that PARylation inhibits BAP1 activity toward nucleosomal H2A-Ub while exerting a stimulatory effect on Ub-AMC. We hypothesized that PARylation restricts the access of BAP1 to nucleosomes, a limitation not applicable to Ub-AMC. Unmodified BAP1 bound to nucleosomes, which was not significantly enhanced by ASXL1^{DEU} (Fig. 6L, lanes 2 and 6; Fig. 6M, lanes 2 and 3). Contrary to our expectations, PARylated BAP1 bound strongly to H2A-Ub nucleosomes regardless of the presence of ASXL1^{DEU}, yet inhibiting H2A deubiquitination (Fig. 6L, lanes 4 and 8). The robust nucleosome binding of BAP1 was not due to histone PARylation, because it still occurred when PARylation was terminated by PARPi before incubation with nucleosomes (Fig. 6M, lane 6).

As observed for Ub-AMC, PARP1 intrinsically stimulated BAP1 activity toward nucleosomal H2A-Ub (Fig. 6G, lane 4; Fig. 6I, lane 3), with this activity increasing proportionally with PARP1 concentration (Fig. 6N). However, PARP1 did not stimulate BAP1 in the absence of ASXL1^{DEU} (Fig. 6L, lane 3), suggesting that it does not play the same role as ASXL1^{DEU} in stimulating BAP1. PARPi treatment did not affect the PARP1 activity for BAP1 stimulation (Fig. 6O) and PARP1 did not significantly increase BAP1 binding to H2A-Ub nucleosomes (Fig. 6L, lanes 3 and 7; Fig. 6M, lane 4), indicating that PARP1 does not activate BAP1 via its catalytic activity or by increasing the BAP1's affinity for H2A-Ub nucleosomes.

The Glu31 PARylation site, frequently mutated in human cancers, promotes BAP1 stability and CPD repair

Next, we investigated the cellular functions of the identified BAP1 PARylation sites. Individual mutation of the eight unambiguous sites to Ala (a non-PARylatable residue) did not noticeably affect either basal or UV-induced PARylation (Supplementary Fig. 7A), suggesting that none of these sites serves as a major PARylation site. Many of BAP1 PARylation sites were mutated in various cancers, among which Glu31 was the most frequently altered, particularly in kidney cancer (Supplementary Fig. 7B). Mutation of Glu31 along with Glu30 to Ala either individually (E30A and E31A) or in combination (E30/31A) had no apparent effects on basal and UV-induced PARylation, probably for the same reason mentioned above (Fig. 7A). Interestingly, these BAP1 mutants exhibited very low protein levels with a significantly shortened half-life, which were fully restored by MG132 treatment (Fig. 7B, C), suggesting that their stability is regulated by ubiquitin-mediated proteasomal degradation. PARPi treatment increased BAP1 polyubiquitination (Fig. 7D) and decreased BAP1 stability in both untreated and UV-treated cells (Fig. 7E, F), suggesting that PARylation at E30/31 stabilizes BAP1 by suppressing its ubiquitination possibly via signaling crosstalk [42]. UV irradiation alone decreased the stability of BAP1 via ubiquitin-mediated degradation (Supplementary Fig. 7C). While exhibiting a low protein level and not rescuing the CPD repair defect in BAP1-depleted cells, E31A was still unable to rescue this defect even when expressed at a level comparable to that of wild-type BAP1 (Fig. 7G, H). These results suggest that Glu31 not only stabilizes BAP1 via PARylation-induced suppression of its degradative ubiquitination but also promotes CPD repair via BAP1 stabilization as well as other mechanisms.

Glu31 participates in promoting CPD repair and reducing the viability of ccRCC cells

Finally, we investigated the clinical significance of Glu31 in BAP1 in ccRCC, the cancer type with the highest frequency of mutations at this site. A database search identified KMRC-20 as the only cell line harboring a missense mutation at Glu31 (altered to Lys, E31K), which exhibited relatively low BAP1 level among the six BAP1-expressing ccRCC cell lines analyzed (Supplementary Fig. 8A). While reexpression of BAP1 in BAP1-depleted KMRC-20 significantly reduced the cell viability, the E31A mutant, exhibiting a low protein level, was defective in this activity even at a level comparable to that of wild-type BAP1 (Fig. 8A, B). We observed similar results for the E31K mutant (Supplementary Fig. 8B, C). BAP1 depletion compromised CPD repair in KMRC-20, and E31A, even at a level comparable to that of wild-type BAP1, did not fully rescue the repair defects after BAP1 depletion (Fig. 8C, D). BAP1 and E31A showed apparently similar levels of basal PARylation, which increased after UV irradiation (Fig. 8E). Similar experiments in UMRC-6 cells, a ccRCC cell line lacking BAP1 expression, showed that BAP1 reduced the cell viability and Glu31 was important for this activity (Fig. 8F, G). Interestingly, in UMRC-6 cells, BAP1 exhibited no activity in promoting CPD repair (Fig. 8H–J), and its PARylation did not significantly increase after UV irradiation (Fig. 8K), suggesting that a BAP1-independent CPD repair pathway may have evolved in this BAP1-null cell line. These results show that Glu31 promotes BAP1 stability and CPD repair activity in ccRCC cells—thus, these functions are cell type-independent—and that it plays an important role in the BAP1-mediated reduction in ccRCC cell viability, and this role appears to be independent of its CPD repair activity.

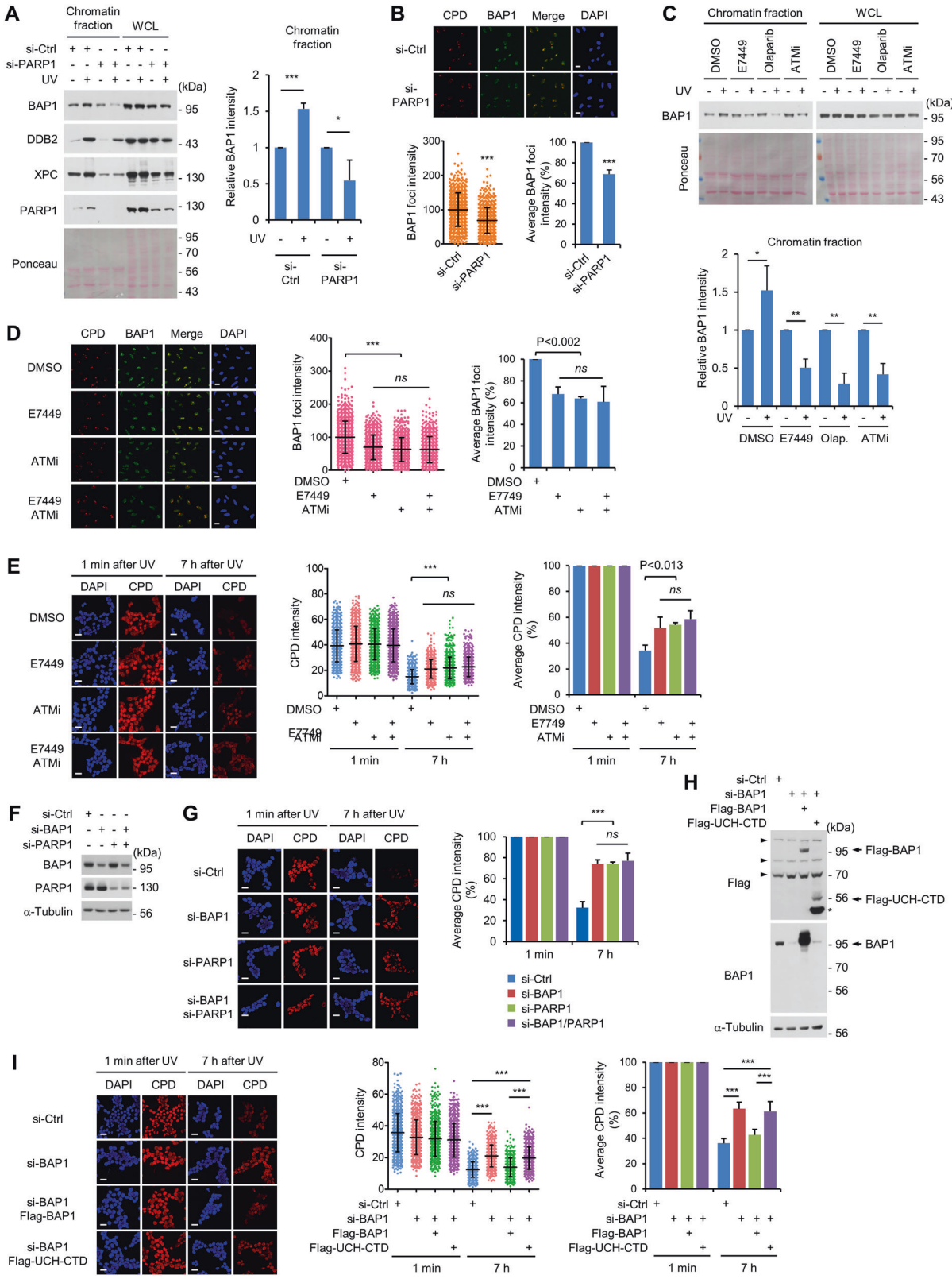

DISCUSSION

Here, we showed that BAP1 promotes the repair of UV-induced DNA damage via its DUB activity. PARP1 interacts with and recruits BAP1 to damage sites immediately after DNA damage, with BAP1 recruitment peaking after DDB2 and XPC. BAP1 recruitment also requires H2A-Ub, which accumulates at damage sites. PARP1 transiently PARylates BAP1 at multiple sites after UV damage and stimulates the DUB activity of BAP1 both intrinsically and via PARylation. Many PARylation sites in BAP1 are altered in multiple cancers, among which Glu31, with particularly frequent mutation in ccRCC, plays a critical role in promoting BAP1 stability via crosstalk between PARylation and ubiquitination for DNA repair

Fig. 4 PARP1 recruits BAP1 to UV damage sites to promote DNA repair. A The effects of PARP1 knockdown on the chromatin binding of BAP1 after UV irradiation (25 J/m^2) were determined by cell fractionation using U2OS cells. The chromatin binding of DDB2, XPC and PARP1 was also analyzed as a control. The intensity of the BAP1 band was quantitated by densitometry and depicted graphically by setting the value for the control lane (−UV) to 1 for each condition. $n = 3$; error bars, mean ± s.d. Images of more gels showing similar results are provided in Supplementary Fig. 4A. **B** Results of the micropore assay showing that PARP1 knockdown reduces BAP1 foci after UV irradiation (25 J/m^2) in U2OS cells. BAP1 foci were quantitated as described in Fig. 1I. The intensity values for BAP1 foci under each condition were pooled from three independent experiments and shown as a scatter plot. Cell counts: 596 and 627 (in the same order as presented in the graph). The percentages of the average BAP1 intensity per each condition are shown as a bar graph. $n = 3$; error bars, mean ± s.d. Scale bar, 20 μm. **C** U2OS cells were treated with a PARPi (E7499 or olaparib, each 10 μM) or an ATMi (10 μM) 30 min before UV irradiation (25 J/m^2) and harvested 60 min later to evaluate the chromatin binding of BAP1 by cell fractionation. PARP1 was also analyzed for comparison. The intensity of the BAP1 band was quantitated by densitometry and depicted graphically by setting the value for the control lane (−UV) to 1. $n = 3$; error bars, mean ± s.d. **D** After treatment with E7499 or ATMi alone or in combination 30 min before UV irradiation (25 J/m^2), U2OS cells were harvested 60 min after UV irradiation to analyze BAP1 foci by a micropore assay. BAP1 foci were quantitated and shown as a scatter plot and a bar graph as described in **B**. Cell counts for the scatter plot: 808, 732, 789, and 760 (in the same order as presented in the graph). $n = 3$; error bars, mean ± s.d. Scale bar, 20 μm. **E** 293T cells were treated with inhibitors and irradiated with UV light as described in **D**, and the efficiency of CPD repair was analyzed and quantitated as described in Fig. 1G. Cell counts: 647, 646, 619, 660, 560, 618, 735, and 667 (in the same order as presented in the graph). $n = 3$; error bars, mean ± s.d. Scale bar, 10 μm. **F** Immunoblot analysis of 293T cells with BAP1 and/or PARP1 knockdown. **G** The knockdown cells described in **F** were irradiated with UV light (25 J/m^2) and analyzed for the efficiency of CPD repair. The percentages of the CPD staining intensity for each condition are depicted graphically. $n = 3$; error bars, mean ± s.d. Scale bar, 10 μm. **H** Immunoblots showing the expression of FL or UCH-CTD-mutant Flag-BAP1 in BAP1-depleted 293T cells. Star, a degraded form of Flag-UCH-CTD; arrowhead, nonspecific band. **I** Results of a CPD repair assay with the cells described in **H**. The data were processed as in **E**. Cell counts: 687, 539, 538, 654, 612, 559, 442, and 534 (in the same order as presented in the graph). $n = 3$; error bars, mean ± s.d. Scale bar, 10 μm.

(Fig. 8L). This study therefore reveals that BAP1 functions in the NER pathway and that PARP1 plays a role as a novel factor that regulates BAP1 enzymatic activity, protein stability, and recruitment to damage sites. Our work also showed that Glu31 participates in reducing the viability of ccRCC cells, likely reflecting its tumor suppressor activity, seemingly via mechanisms independent of DNA repair.

H2A-Ub stimulates the repair of UV-induced DNA damage, for example, by inducing modulation of chromatin structure and the assembly of repair proteins at DNA lesions [43–47]. Our data show that H2A-Ub functions to recruit BAP1 to damage sites, providing additional example for the role of H2A-Ub in repair protein recruitment. This role of H2A-Ub may be inconsistent with the fact that BAP1 requires its DUB activity to stimulate DNA repair. One possible scenario would be that, after recruited to damage sites via H2A-Ub, BAP1 could in turn target H2A-Ub and fine-tune its levels to regulate damage-site recruitment of itself and DNA repair. Chromatin remodelers, such as INO80, are recruited to UV damage sites to promote repair via their activity to modulate chromatin structure [48, 49]. BAP1 interacts with and recruits INO80 to replication forks for both normal DNA synthesis and replication stress recovery [34, 35]. Therefore, after recruitment by PARP1, BAP1 may in turn recruit INO80 to damage sites to promote DNA repair.

Although our data showed that PARP1 recruits BAP1 to damage sites, whether PARylation contributes to this process is currently unclear. However, we predict that neither PARP1 auto-PARylation nor PARP1-mediated BAP1 PARylation is important for BAP1 recruitment, based on our results that the central modification domain of PARP1 is dispensable for BAP1 binding and that PARPi treatment has no effect on the interaction between BAP1 and PARP1. In support of this hypothesis, BAP1 does not directly interact with PAR polymers in an in vitro binding study [37]. Thus, PARP1 likely recruits BAP1 to DNA damage sites by a direct protein-protein interaction rather than via PAR-mediated protein binding.

Our results suggest that PARP1 promotes BAP1 stability via crosstalk between PARylation and ubiquitination and that the Glu30/31 PARylation sites play a critical role in this activity. The PAR chains on Glu30/31 may block recruitment of E3 ligases to BAP1 to prevent its proteasomal degradation. This finding therefore adds BAP1 to the list of proteins whose stability is controlled by crosstalk between PARylation and ubiquitination. Interestingly, while the E31A mutant exhibits low stability, it is still defective in promoting CPD repair even at a level comparable to that of wild-type BAP1, suggesting that PARylation at Glu31 plays an additional role in CPD repair beyond protein stabilization. As PARylation stimulates BAP1 activity, one possibility is that PARylation of Glu31 mediates this effect.

Intriguingly, while PARP1 stimulates BAP1 activity toward Ub-AMC and further enhances this activity by PARylation, it stimulates BAP1 toward H2A-Ub nucleosomes and completely inhibits this activity by PARylation, accompanied by strong BAP1 binding to the nucleosomes. We propose that PARP1 stimulates BAP1 both intrinsically and via PARylation, probably by allosterically affecting the intrinsic activity of BAP1. Regarding the activity of PARylated BAP1 toward nucleosomal H2A, an unproductive complex could form with strong affinity, rendering H2A-Ub untargetable. Formation of this complex may be an artifact of the in vitro reaction or could truly occur in vivo as a mechanism to inhibit H2A deubiquitination. Alternatively, PARylation may stimulate BAP1 activity toward nucleosomal H2A with the assistance of additional factors in vivo. Regardless of the mechanisms, these activities of PARP1 toward BAP1 may reflect the complexity of their control over CPD repair in the context of chromatin substrates.

The activity of BAP1 in maintaining genome stability can account for its tumor suppressor function [14]. Since this activity of BAP1 is attributed to its functions in DSB repair and DNA replication under normal and stress conditions, our work revealing the role of BAP1 in NER supports the proposed mechanism. Although DNA repair activity of BAP1 has been suggested to enable synthetic lethal approach using PARPis for the treatment of cancers with BAP1 mutations, recent clinical studies showed that PARP inhibition does not selectively target BAP1 deficient mesothelioma [50–52]. Given that synthetic lethality relies on the inhibition of pathways upon which DDR-deficient cancer cells have become dependent for their survival, the intimate link of BAP1 and PARP1 in DNA repair, functioning in the same pathway, could be a potential reason for the poor clinical outcomes. Therefore, alternative synthetic lethal strategies will be necessary for the treatment of BAP1 deficient cancers, for example, targeting PARP1-independent DDR pathways.

Recent studies suggested that the activity of BAP1 to regulate cell death also accounts for its tumor suppressor function [53–56]. For example, fibroblasts derived from heterozygous *BAP1* mutation carriers with BAP1 cancer syndrome accumulated more DNA damage after UV exposure due to a reduced DNA repair ability compared to wild-type fibroblasts. These mutant cells, however, were resistant to apoptosis, resulting in increased cell survival after DNA damage, suggesting that a decrease in the BAP1 level

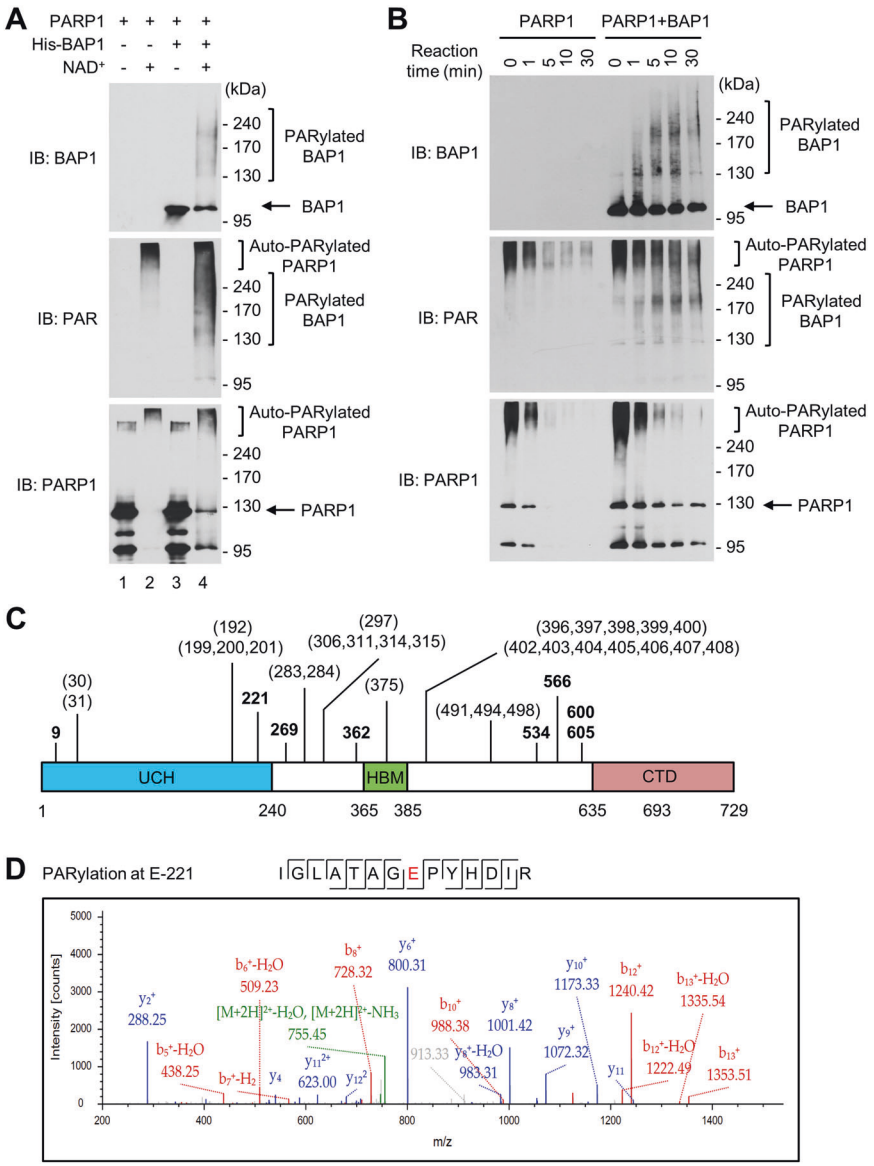

Fig. 5 PARP1 PARylates BAP1 at multiple sites in vitro. A PARP1 alone or in combination with His-BAP1 was incubated in the absence or presence of NAD^+, and the reactions were subjected to SDS-PAGE and immunoblotting as indicated. PARylated BAP1 and auto-PARylated PARP1 are indicated. Note that most auto-PARylated PARP1 disappeared because it did not enter the resolving gel (see also Supplementary Fig. 5B, C). **B** BAP1 was incubated with PARP1 in the presence of NAD^+, and the reactions were terminated at the indicated times before SDS-PAGE and immunoblotting. **C** Summary of the PARylation sites in BAP1. BAP1 and PARP1 were incubated in the presence of NAD^+, and the reactions were subjected to LC-MS/MS analysis. The numbers in bold indicate unambiguously identified PARylation sites, and those in parentheses indicate ambiguous sites. **D** The MS/MS spectra of the PARylation site at Glu221 (E in red) are shown as a representative example. The MS/MS spectra of all identified PARylation sites in BAP1 are summarized in Supplementary Material.

contributes to cellular transformation by leading to enhanced DNA damage and reduced apoptosis [53]. Therefore, our finding of the BAP1 activity for UV-induced DNA damage repair in primary melanocytes can explain why melanomas and skin cancers—often caused by UV radiation—are prevalent, although almost every tumor type has been reported in carriers of germline *BAP1* mutations.

MATERIALS AND METHODS

Cell culture

The HEK-293T (293T), U2OS, UMRC-6, UMRC-3, HK-2, A704, 786-O and Caki-2 cell lines were purchased from ATCC (Manassas, VA). The KMRC-20 cell line (JCRB1071) was purchased from the JCRB Cell Bank (Japan). 293T, UMRC-6, UMRC-3, HK-2, A704 and KMRC-20 cells were cultured in Dulbecco's modified Eagle's medium supplemented with 10% fetal bovine serum (FBS) (Gibco, Carlsbad, CA), 100 U/mL penicillin, and 100 µg/mL streptomycin. U2OS and Caki-2 cells were cultured in McCoy's 5A medium supplemented with 10% FBS, 100 U/mL penicillin and 100 µg/mL streptomycin. 786-O cells were cultured in RPMI 1640 medium supplemented with 10% FBS, 100 U/mL penicillin, and 100 µg/mL streptomycin. Normal human primary epithelial melanocytes from adult donors (HEMa, PCS-200-013) were purchased from ATCC and cultured according to the vendor's instructions in Dermal Cell Basal Medium (PCS-200-030) supplemented with Adult Melanocyte Growth Kit components (PCS-200-042) and 10 U/mL penicillin plus 10 µg/mL streptomycin. All cells were maintained at 37 °C in a humidified incubator with 5% CO_2. The cell lines were authenticated with DNA fingerprinting using STR (short tandem repeat) markers every 50 passages and were tested for the absence of *Mycoplasma* contamination using the e-Myco VALiD Mycoplasma PCR Detection Kit (Intron Biotechnology).

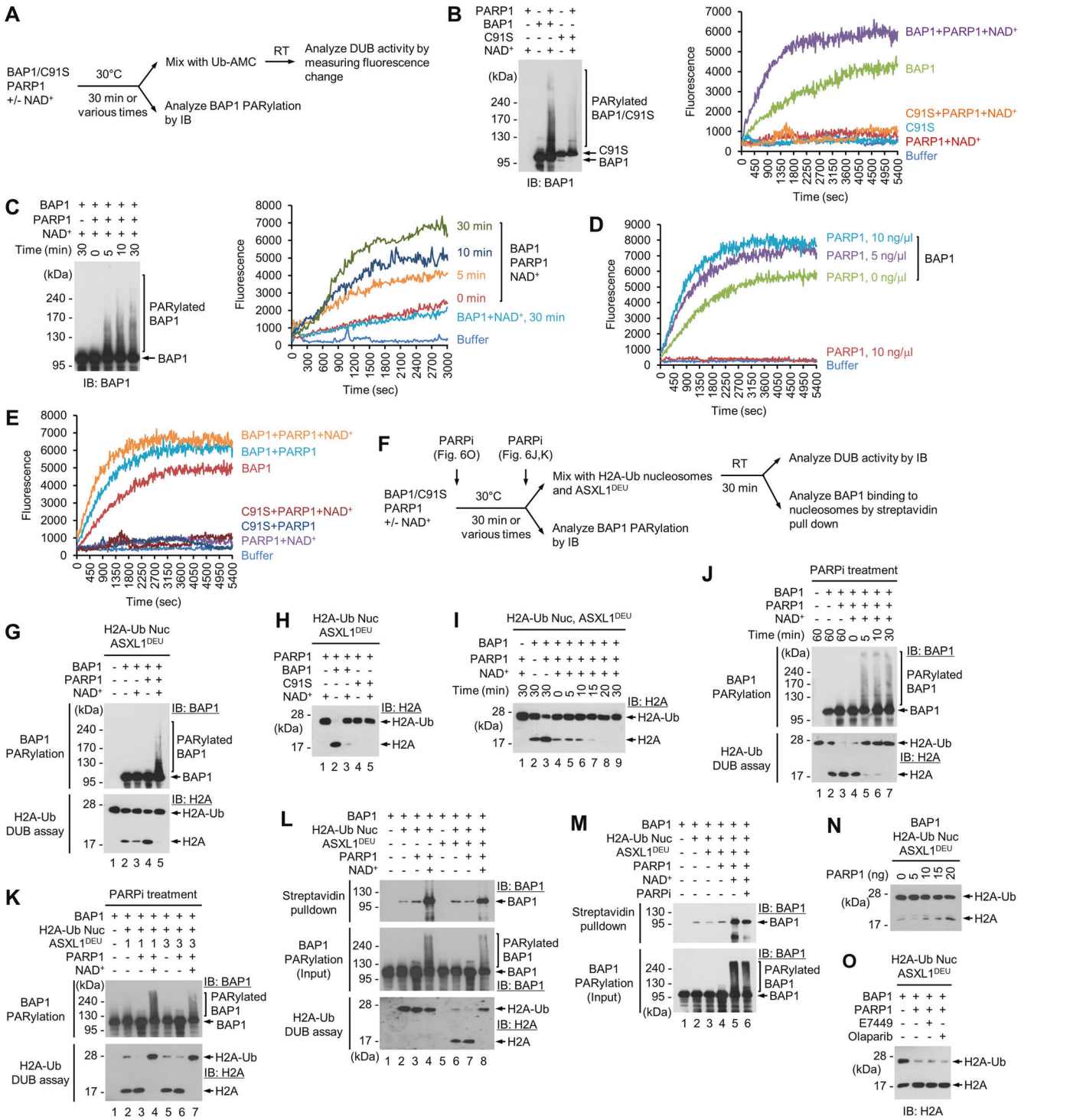

UV irradiation

For induction of global UV damage, cells were washed with PBS and exposed to the indicated doses of UV using a UV crosslinker (UVP, LC-1000). For local UV irradiation in the micropore assay, cells were washed with PBS and exposed to UV irradiation through an Isopore polycarbonate filter (Millipore) with a pore size of 5 µm.

Inhibitor treatment

E7449 (Selleckchem, S8419), olaparib (Selleckchem, S1060) and KU-55933 (MedChemExpress, HY-12016), all dissolved in DMSO, were added to culture media at a final concentration of 10 µM 30 min prior to UV irradiation where applicable.

Antibodies

The primary antibodies used in this work were as follows: anti-BAP1 (mouse IgG, sc-28383; rabbit IgG, sc-28236), anti-XPC (mouse IgG, sc-74410), anti-PARP1 (sc-8007), anti-c-Myc (rabbit IgG, sc-789), anti-α-tubulin (sc-8035), anti-Ha (sc-7392) and anti-actin (sc-8432) purchased from Santa Cruz; anti-Poly/Mono-ADP ribose (E6F6A) (rabbit IgG, #83732) and anti-phospho-BAP1-S592 (#9373) obtained from Cell Signaling Technology; anti-Flag (F3165) obtained from Sigma; anti-c-Myc (mouse IgG, SA-294) and anti-PAR (mouse IgG, ALX-804-220) obtained from Enzo Life Sciences; anti-CPD (CAC-NM-DND-001) and anti-6-4PP (CAC-NM-DND-002) obtained from Cosmo Bio; anti-H2A (07-146) and anti-H2A-Ub (05-678) obtained from Millipore; anti-GAPDH (LF-PA0212)

Fig. 6 PARP1 regulates the catalytic activity of BAP1 intrinsically and via PARylation. A Experimental scheme for the PARylation-coupled Ub-AMC DUB assay. **B** PARylation reactions containing the components as indicated were incubated for 30 min at 30 °C and divided into two equal parts, one of which was used to analyze BAP1 PARylation by immunoblotting (left) and the other used for an Ub-AMC DUB assay (right). Note that wild-type BAP1 migrates slightly faster than BAP1-C91S on the gel because the former contains only a His tag, whereas the latter contains both His and Flag tags. **C** The indicated PARylation reactions were incubated for various times at 30 °C and were then divided into two equal parts and processed as described in **B**. **D** BAP1 was incubated alone or with increasing concentrations of PARP1 for 5 min at RT, and the reaction was subjected to a Ub-AMC DUB assay. The reaction with only PARP1 was included as a control. **E** Results of the Ub-AMC DUB assays of the indicated reactions. **F** Experimental scheme for the PARylation-coupled H2A-Ub nucleosome DUB assay and streptavidin pulldown. **G** PARylation reactions were divided into two equal parts, one of which was used to analyze BAP1 PARylation as described in **B**. The other half was further incubated with H2A-Ub nucleosomes and $ASXL1^{DEU}$ for 30 min at RT and was then used to analyze H2A deubiquitination by immunoblotting. **H** Results of the DUB assays with H2A-Ub nucleosomes for the indicated PARylation reactions. **I** Results of the H2A-Ub nucleosome DUB assay showing that PARylation of BAP1 decreases its DUB activity with reaction time. **J** PARylation reactions were performed as indicated, terminated by the addition of a PARPi and divided into two equal parts before being processed as described in **G**. **K** PARylation-coupled H2A-Ub nucleosome DUB assay similar to that described in **J** showing that excessive $ASXL1^{DEU}$ does not alleviate the inhibition of H2A deubiquitination by PARylated BAP1. The numbers in the $ASXL1^{DEU}$ row indicate the relative amounts of $ASXL1^{DEU}$ added to the reactions. **L** PARylation reactions were performed as indicated and divided into three parts. The first two parts were used to determine BAP1 PARylation and H2A deubiquitination as described above. The third part was used for a streptavidin pulldown assay to analyze the amount of BAP1 bound to H2A-Ub nucleosomes. **M** Experiments similar to those described in **L** showing that treatment of the PARylation reactions with a PARPi before incubation with H2A-Ub nucleosomes and $ASXL1^{DEU}$ has no effect on BAP1 binding to the nucleosomes. **N** PARP1 itself stimulates BAP1 activity toward H2A-Ub nucleosomes. BAP1 was incubated with increasing concentrations of PARP1 in the presence of H2A-Ub nucleosomes and $ASXL1^{DEU}$, and H2A deubiquitination was analyzed by immunoblotting. **O** Results of experiments similar to those described in **N** showing that PARPi treatment has no effect on PARP1-mediated stimulation of BAP1 activity toward H2A-Ub nucleosomes.

obtained from AbFrontier; and anti-DDB2 (rabbit IgG, 181136) obtained from Abcam.

Transfection, siRNAs and plasmids

Transfections with plasmids and synthetic siRNAs were performed using polyethylenimine (PEI) and Lipofectamine RNAiMAX (Invitrogen), respectively. The siRNA sequences used were as follows: si-BAP1, 5′-cuc cau cag acc aau cca auu-3′; si-Ring1A, 5′-cug cau uca gaa cuc aug u(dTdT); si-Ring1B, 5′-ccu agu aac aaa cgg acc a(dTdT); si-PARP1, 5′-gga ggg ucu gau gau agc auu-3′; and si-control, 5′-ccu acg cca cca auu ucg uuu-3′. The plasmid vectors expressing full-length and truncated Flag-BAP1, as well as those expressing full-length Myc-BAP1, have been described previously [34]. The expression vector for Flag-UCH-CTD was generated by a PCR-based sequence deletion method in which the primers were placed outside of the region to be deleted to obtain a linear sequence that was ligated into a circular plasmid. The oligo sequences used were as follows: 5′-agc cca gtg gag aag gag gtc gtg gaa gcc ac, and 5′-ctt gat cct gcg gtc ggg cac cac tgc cat c. The expression vectors for full-length and truncated Myc-PARP1 (ΔBRCT, DBD-ART, DBD, and ΔHD/ART) were constructed by cloning the corresponding sequences amplified by PCR from pQCXIH-PARP1-His_6/FLAG into the pcDNA3.1/Myc-His(-) vector and HD/ART into the pCMV-Myc-NLS vector. The vectors expressing GFP-BAP1, BAP1-GFP and PARP1-GFP were constructed by cloning the corresponding sequences into pEGFP-C2, pcDNA3-EGFP, and pEGFP-N1, respectively. The bacterial expression vectors for His-Flag-BAP1, His-Flag-BAP1-C91S and the DEUBAD domain of ASXL1 ($ASXL1^{DEU}$; amino acid positions 238–390) were constructed by cloning the corresponding PCR products into the EcoRI and SalI sites in pET-21a. The vectors expressing siRNA-resistant Flag-BAP1 and Flag-BAP1-C91S, the vectors expressing Flag-BAP1-A592/D592/E529, and the vectors expressing the series of non-PARylatable Flag-BAP1 mutants (E9A, E30A, E31A, E30/31A, E221A, E269A, D362A, E534A, E566A, E600A, and E605A) were constructed with a QuikChange Site-Directed Mutagenesis Kit (Stratagene) with specific oligonucleotides. The lentiviral vectors expressing Flag-BAP1 and Flag-BAP1-C91S were described previously [34]. The lentiviral vector expressing Flag-BAP1-E31A was constructed by introducing the mutation into the Flag-BAP1 lentiviral vector with the QuikChange Site-Directed Mutagenesis Kit (Stratagene) with specific oligonucleotides. The oligonucleotide sequences used for PCR and site-directed mutagenesis are available upon request. All plasmid constructs and mutations generated in this work were verified by sequencing.

Immunoprecipitation (IP)

Cells were lysed by incubation in NETN buffer (20 mM Tris-Cl (pH 8.0), 150 mM NaCl, 1 mM EDTA (pH 8.0), 0.5% NP-40, 0.5 mM PMSF, 10 mM NaF, and protease inhibitor cocktail) on ice for 30 min followed by sonication using a Cole-Parmer Ultrasonic Homogenizer (30% amplitude, three times, 10 s each). The lysates were clarified by centrifugation at 13,000 rpm for 10 min at 4 °C and precleared by incubation with Protein G agarose (Millipore) for 2 h at 4 °C. After centrifugation, the supernatants were incubated with anti-Flag M2 Affinity Gel (Sigma) for IP of Flag-BAP1 or with the indicated primary antibodies for IP of other proteins overnight at 4 °C. For all antibody incubations, protein G agarose was added and further incubated for 4 h at 4 °C. The precipitated beads were intensively washed with NETN buffer and boiled for 5 min in SDS sample loading buffer before SDS-PAGE and immunoblot analysis.

Identification of BAP1-interacting proteins by mass spectrometry (MS)

293T cells expressing Flag-BAP1 were mock-treated or irradiated with UV light (50 J/m^2) 1 h before harvesting. Cells were lysed in NETN buffer, and the lysates were clarified by centrifugation at 13,000 rpm for 10 min at 4 °C. The supernatants were incubated with anti-Flag M2 Affinity Gel overnight at 4 °C. The beads were washed several times with NETN buffer, suspended in SDS sample loading buffer, and boiled for 5 min. Samples were subjected to SDS-PAGE and visualized by silver staining. The band of interest was excised and subjected to trypsin digestion and MALDI-TOF analysis by essentially the same method described previously in the MS core facility at Ewha Womans University [57].

Immunoblot (IB) analysis

Whole-cell lysates were prepared in RIPA buffer (50 mM Tris-Cl (pH 8.0), 150 mM NaCl, 0.5% sodium deoxycholate, 0.1% SDS, 1% NP-40, 0.5 mM PMSF, 10 mM NaF, and protease inhibitor cocktail), and protein concentrations were determined by a BCA assay (Pierce). Protein samples were mixed with SDS sample loading buffer and boiled for 5 min. SDS-PAGE and immunoblot analysis were conducted according to standard procedures. Histone extraction and immunoblot analysis were performed as previously described [58]. Full-length original western blots for the results are provided in Supplementary materials.

Cell fractionation

Cell fractionation was performed according to the procedures provided by the Shah group [59]. Because we observed that UV-induced chromatin association of BAP1 was more evident in the pellet than in the chromatin extract and that DDB2 and XPC clearly exhibited UV-induced chromatin binding in both the chromatin extract and the pellet (Supplementary Fig. 1B), we used the pellet as the chromatin-bound fraction for BAP1 as well as DDB2 and XPC for convenience. In brief, cells were lysed in Buffer A for 7 min at 4 °C and centrifuged at 1000 × *g* for 5 min at 4 °C. The pellet was washed with Buffer A and suspended in Buffer B for 30 min at 4 °C before centrifugation at 16,000 × *g* for 30 min at 4 °C. The pellet was then incubated in Buffer C containing benzonase (25 U/mL) for 40 min at RT, and the reaction was stopped with 5 mM EGTA and 5 mM EDTA before centrifugation at 16,000 × *g* for 10 min. The pellet was suspended in SDS sample loading buffer and boiled for 5 min.

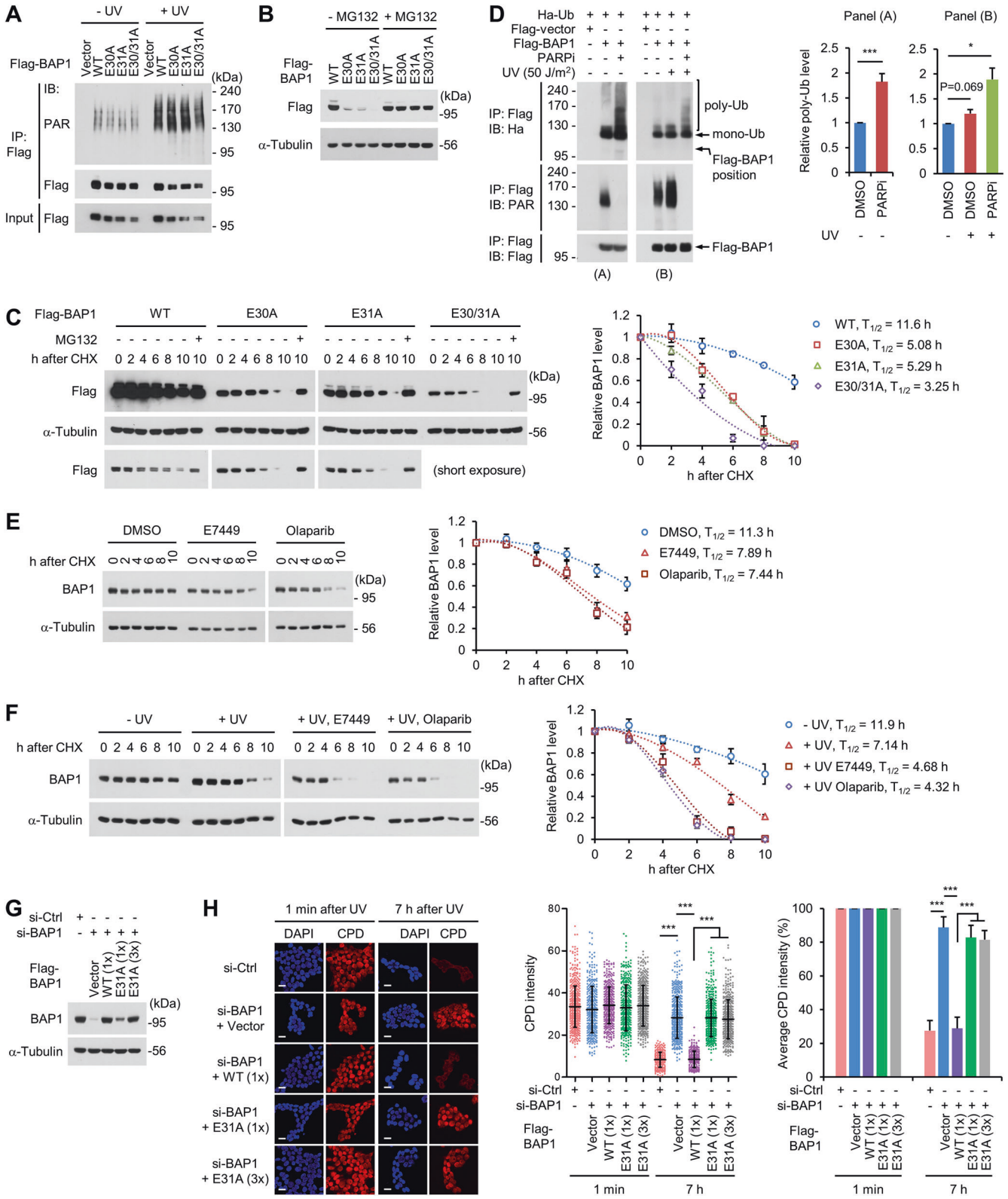

Colony formation assay

Colony formation assay was performed as previously described [60]. 293T cells transfected with nontargeting or BAP1-specific siRNAs for 24 h were seeded into 6-well plates (7×10^2 cells per well) in triplicate, irradiated with the indicated doses of UV light, and incubated for 8 days. Visible colonies of more than 50 cells were counted.

DNA repair assay

Cells were fixed on coverslips with 4% paraformaldehyde for 10 min and permeabilized with 0.5% Triton X-100 in PBS for 10 min. After rinsing with PBS, the cells were incubated in 2 M HCl for 30 min at room temperature (RT) to denature DNA. After several washes with PBS, the cells were blocked with 4% BSA in PBS and incubated with primary antibodies

Fig. 7 The Glu31 PARylation site, frequently mutated in human cancers, promotes BAP1 stability and CPD repair. A Results of the in vivo PARylation assay for the E30A, E31A and E30/31A mutants of Flag-BAP1 before and 30 min after UV irradiation (25 J/m^2) in 293T cells. **B** 293T cells were transfected with the indicated expression vectors, treated with MG132 (10 μM) for 6 h, and harvested for immunoblotting. **C** After transfection with the indicated vectors, 293T cells were treated with cycloheximide (CHX) and harvested at various time points for immunoblotting. The last lane for each condition was cotreated with CHX and MG132 for 10 h. The intensities of the Flag-BAP1 bands were quantitated by densitometry and depicted graphically by setting the value for the first lane of each condition to 1 after normalization to tubulin. The half-life ($T_{1/2}$) of Flag-BAP1 for each condition is shown. $n = 3$; error bars, mean ± s.d. **D** PARP inhibition increases BAP1 polyubiquitination. After cotransfection with Flag-BAP1 and Ha-Ub, 293T cells were pretreated with a PARPi and MG132 and irradiated with UV light (25 J/m^2) where indicated. Cell lysates were prepared after 30 min, and Flag-tagged proteins were immunoprecipitated and analyzed for Ha-Ub and PAR by immunoblotting. The intensity of the polyubiquitinated Flag-BAP1 band was quantitated by densitometry and depicted graphically by setting the value for the control lane (without PARPi or DMSO) to 1. **E** Results of CHX chase experiments similar to those described in **C** to determine the effects of PARPi treatment on the stability of endogenous BAP1. Quantitation was performed as described in **C**. $n = 3$; error bars, mean ± s.d. **F** Results of CHX chase experiments similar to those described in **C** to determine the effects of PARPi treatment on the stability of endogenous BAP1 after UV irradiation (50 J/m^2). Quantitation was performed as described in **C**. $n = 3$; error bars, mean ± s.d. **G** 293T cells were cotransfected with BAP1 siRNA and the indicated Flag-BAP1 expression vectors and were then subjected to immunoblotting with an anti-BAP1 antibody. The relative amounts of transfected vector DNA are indicated. **H** After transfection as described in **G**, 293T cells were irradiated with 25 J/m^2, harvested immediately or 7 h later, and subjected to a CPD repair assay. Quantitation and analysis were performed as described in Fig. 1G. Cell counts: 505, 371, 422, 379, 464, 340, 505, 320, 468, and 435 (in the same order as presented in the graph). $n = 3$; error bars, mean ± s.d. Scale bar, 10 μm.

against CPD and 6-4PP in PBS with 1% BSA for 1 h at RT. The cells were washed four times with PBS containing 0.05% Tween 20 and incubated for 30 min at RT with Alexa Fluor 568 goat anti-mouse IgG. After washing, the cells were mounted using VECTASHIELD Mounting Medium with DAPI (Vector Laboratories). Cell images were acquired using a Carl Zeiss LSM 880 confocal laser scanning microscope and processed using ZEN 2.3 software (Carl Zeiss). The CPD staining intensity was measured by ImageJ.

Micropore assay

After local UV irradiation, cells were washed with PBS and treated with ice-cold cytoskeleton (CSK) buffer (0.5% Triton X-100, 100 mM NaCl, 300 mM sucrose, 10 mM PIPES (pH 6.8), 3 mM $MgCl_2$, and 1 mM EGTA) for BAP1 and H2A-Ub staining for 4 min. This step was necessary for BAP1 and H2A-Ub staining likely due to their tight association with chromatin, but not needed for DDB2 and XPC staining. The cells were fixed with methanol on ice for 10 min, blocked with 3% BSA in PBS for 1 h, and incubated first with the appropriate primary antibody in PBS for 16 h at 4 °C and subsequently with the corresponding secondary antibody (Alexa Fluor 488 goat anti-mouse IgG for BAP1 and XPC; Alexa Fluor 488 goat anti-rabbit IgG for DDB2) in PBS for 30 min at RT. The cells were then stained for CPD, and confocal images were acquired as described before. The intensity of the protein foci was calculated by quantifying the area of CPD foci and normalizing to the background value for each cell using the ZEN 2.3 software.

In vitro pulldown assay

His-BAP1 (Boston Biochem) was first immobilized on Ni-NTA beads, washed with buffer containing 20 mM Tris-Cl (pH 8.0), 150 mM NaCl, and 1% NP-40, and then incubated with recombinant PARP1 (Trevigen) for 2 h. The beads were intensively washed with buffer containing 20 mM Tris-Cl (pH 8.0), 150 mM NaCl, 1% NP-40, and 80 mM imidazole and boiled for 5 min in SDS sample loading buffer before SDS-PAGE and immunoblot analysis.

Expression and purification of recombinant proteins

The vectors expressing His-ASXL1^{DEU}, His-Flag-BAP1 and His-Flag-BAP1-C91S were transformed into *E. coli* BL21, and protein expression was induced by 0.2–0.5 mM Isopropyl β-d-1-thiogalactopyranoside (IPTG; at an optical density (OD) of 0.6) at 30 °C for 5 h. After lysis with lysis buffer (50 mM NaH_2PO_4, 200 mM NaCl, 10 mM imidazole, and 1% NP40), lysates were incubated with Ni-NTA agarose beads (Trevigen) and loaded onto a Poly-Prep chromatography column (-Bio-Rad). After washing with wash buffer (50 mM NaH_2PO_4, 300 mM NaCl, and 20 mM imidazole), proteins were eluted using elution buffer (50 mM NaH_2PO_4, 300 mM NaCl, and 250 mM imidazole). Proteins were dialyzed with dialysis buffer (20 mM Tris-Cl (pH 8.0), 100 mM NaCl, 20% glycerol, and 1 mM dithiothreitol (DTT)) and stored in aliquots at −80 °C.

Ub-AMC DUB assay

The DUB activity of BAP1 was measured with a ubiquitin 7-amido-4-methylcoumarin (Ub-AMC) DUB assay system (Boston Biochem) according to the manufacturer's instructions. Reactions were carried out in black 96-well plates at RT, and fluorescence signals were measured every 15 s using a SpectraMax i3X microplate reader (I3X-SC-ACAD, Molecular Devices) at an excitation wavelength of 350 nm and an emission wavelength of 455 nm.

DUB assay with H2A nucleosomes

10 μL of BAP1 PARylation reactions were mixed with 10 μL of DUB buffer (50 mM Tris-Cl (pH 7.5), 50 mM $NaCl_2$, 1 mM $MgCl_2$, and 1 mM DTT) containing 100 ng of ASXL1^{DEU} and 500 ng of H2A-Ub mononucleosomes (containing H2A-K119-Ub and a 5′ biotin-TEG group, EpiCypher), and incubated at RT for 90 min. Reactions were terminated by the addition of 7 μl of 4× SDS sample loading buffer and boiling for 5 min before SDS-PAGE and immunoblot analysis. ASXL1^{DEU} activates BAP1 by increasing its affinity for the ubiquitin moiety of H2A [61].

In vitro PARylation assay

Total reaction volumes of 20 μL containing 100 ng of His-BAP1 (Boston Biochem) and 400 ng of PARP1 (Trevigen) in buffer (20 mM HEPES (pH 7.5), 50 mM NaCl, 20 mM $MgCl_2$, 40 μg/mL activated DNA (Trevigen), 4 mM NAD^+ (Trevigen) and 1 mM DTT) were incubated for 30 min at 30 °C. Where indicated, His-Flag-BAP1 and His-Flag-BAP1-C91S were also used in the reactions. Reactions were terminated by adding SDS sample loading buffer and boiling for 5 min before SDS-PAGE and immunoblot analysis.

Streptavidin pulldown assay

Total reaction volumes of 30 μL containing 150 ng of His-BAP1 and 600 ng of PARP1 in PARylation reaction buffer were incubated at RT for 30 min. ASXL1^{DEU} (150 ng) and H2A-Ub mononucleosomes (500 ng) were added to the reactions and incubated at RT for 15 min. These reactions were mixed with 800 μL of a buffer containing 1% NP-40 and 30 μL of streptavidin agarose (Novagen, 69203) and incubated at 4 °C overnight. The next day, the beads were washed three times with reaction buffer containing 1% NP-40 by centrifugation at 1000 × *g* for 3 min. After the supernatants were discarded, 20 μL of SDS sample buffer was added to the beads, which were boiled for 10 min and subjected to SDS-PAGE and immunoblot analysis.

In vivo PARylation assay

After transfection of 293T cells with Flag-BAP1, Flag-BAP1 was immunoprecipitated from cell lysates under denaturing conditions (to remove associated proteins) as previously described with some modifications [62]. In brief, cells were lysed in buffer containing 25 mM Tris-Cl (pH 8.0) and 1% SDS on ice for 30 min. Lysates were sonicated to fragment the DNA and clarified by centrifugation. The resulting supernatants were diluted 10-fold in EB300 (50 mM Tris-Cl (pH 8.0), 300 mM NaCl, 1% NP-40, and 10 mM β-mercaptoethanol) and incubated overnight with the primary antibody and protein G agarose. The beads were intensively washed with EB300 and boiled for 5 min in SDS sample loading buffer. After electrophoretic separation of the proteins in the samples, PARylation of Flag-BAP1 was detected by immunoblotting using an anti-PAR antibody.

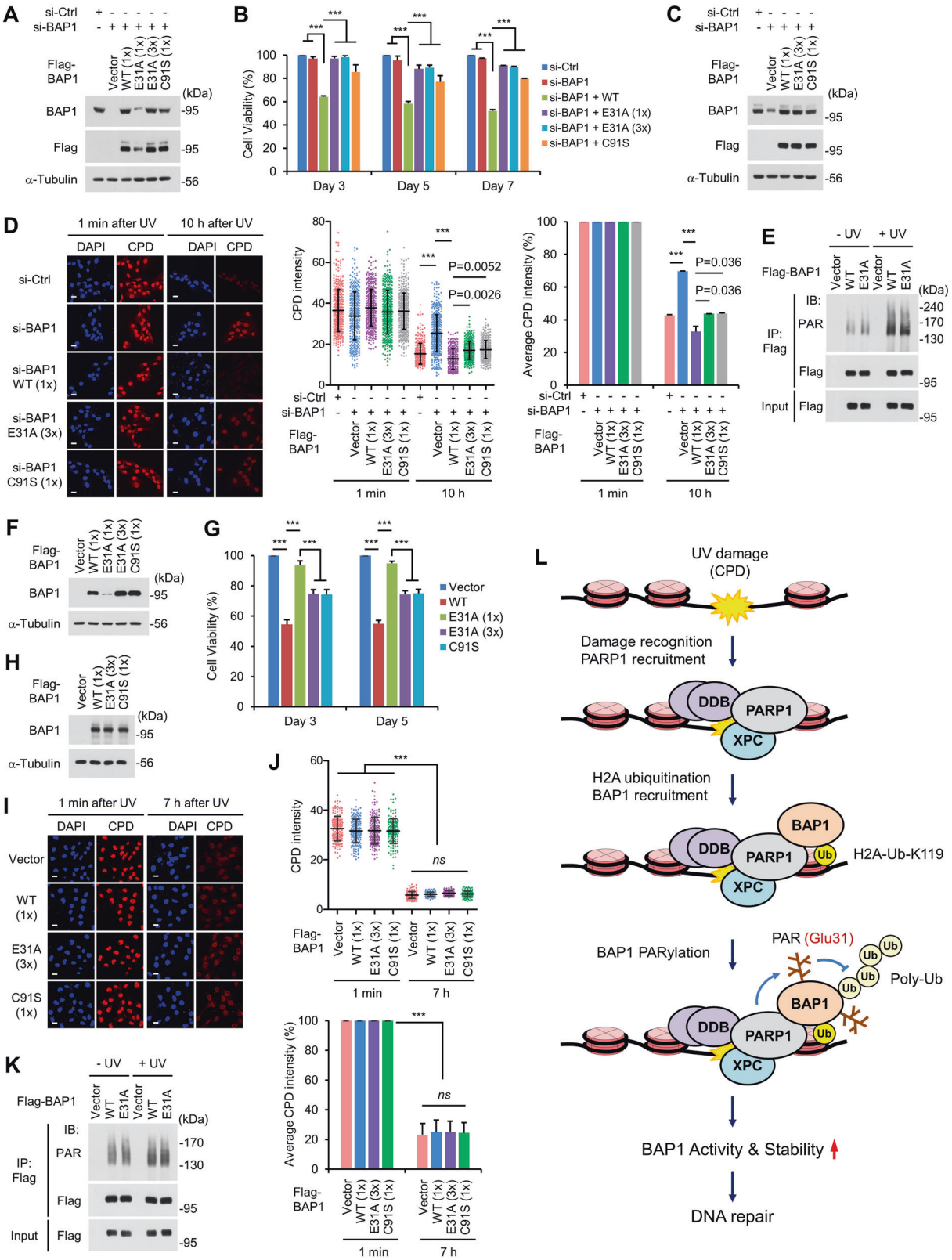

In vivo ubiquitination assay

The in vivo ubiquitination assay was performed under denaturing conditions as previously described [63]. Cells were suspended in 1% SDS lysis buffer containing 1% SDS, 5 mM EDTA (pH 8.0), 10 mM β-mercaptoethanol, 10 mM NaF, and protease inhibitor cocktail (0.5 mM PMSF, 50 μg/mL pepstatin A, 5 μg/mL leupeptin, and 5 μg/mL aprotinin) and incubated for 10 min at 4 °C. Lysates were boiled for 5 min at 95 °C and sonicated using a Branson Sonifier 450 Sonicator (10-s pulses for 2 min). Lysates were clarified by centrifugation at 16,000 × *g* for 20 min at 4 °C. The supernatants were diluted 10-fold in RIPA buffer (50 mM Tris-Cl (pH 8.0), 150 mM NaCl, 0.5% sodium deoxycholate, 0.1% SDS, 1% NP-40, 10 mM NaF, and protease inhibitor cocktail) to reduce the SDS concentration to 0.1% and were then incubated with anti-Flag M2

Fig. 8 BAP1 Glu31 promotes CPD repair and reduces the viability of ccRCC cells. A After transfection with BAP1 siRNA, KMRC-20 cells were transduced with lentiviral vectors expressing the indicated Flag-BAP1 protein and analyzed for BAP1 expression by immunoblotting. The relative volumes of the virus-containing medium used for transduction are indicated. **B** At various days after lentiviral transduction as described in **A**, KMRC-20 cells were evaluated for viability by an MTS assay. $n = 3$ (each performed with triplicates); error bars, mean ± s.d. **C** Results of immunoblotting similar to that described in **A** for the CPD repair assay. **D** After lentiviral transduction as described in **C**, KMRC-20 cells were irradiated with 50 J/m^2 and subjected to a CPD repair assay. Quantitation and analysis were performed as in Fig. 1G. Cell count: 391, 369, 433, 377, 466, 345, 438, 318, 365, 382 (in the same order as presented in the graph). Scale bar, 20 μm. **E** Results of the in vivo PARylation assay for Flag-BAP1 and Flag-E31A before and after UV irradiation (50 J/m^2) in KMRC-20 cells. **F** UMRC-6 cells were transduced with the lentiviral vectors for the indicated Flag-BAP1 and analyzed for BAP1 expression by immunoblotting. The relative volumes of the virus-containing medium used for transduction are indicated. **G** Results of the MTS assay for UMRC-6 cells after lentiviral transduction as described in **F**. $n = 3$ (each performed in triplicate); error bars, mean ± s.d. **H** Results of immunoblotting similar to that in **F** for the CPD repair assay. **I**, **J** After lentiviral transduction as described in **H**, UMRC-6 cells were irradiated with 50 J/m^2 and subjected to a CPD repair assay. Quantitation and analysis were performed as in Fig. 1G. Cell counts: 176, 185, 190, 158, 179, 161, 157, and 160 (in the same order as presented in the graph). Scale bar, 20 μm. **K** Results of the in vivo PARylation assay for Flag-BAP1 and Flag-E31A before and after UV irradiation (50 J/m^2) in UMRC-6 cells. **L** Model for the role of BAP1 and its regulation by PARP1 during NER. See text for the details.

Affinity Gel. The beads were precipitated and washed intensively before SDS PAGE and immunoblot analysis.

Hydroxylamine treatment of PARylated BAP1 protein

The PARylation reaction mixture (40 μL) was divided in half by volume. The first half was resolved by 12% SDS-PAGE until the tracking dye had migrated nearly 1.5 cm into the resolving gel. This short run lane was further divided into four gel bands and minced into smaller gel pieces. Proteins in the destained gel pieces were reduced using DTT (10 mM, 56 °C, 45 min) and alkylated using iodoacetamide (IAM; 55 mM, RT, 30 min in the dark). Next, the gel pieces were washed, dehydrated and soaked in 0.5 M hydroxylamine (Sigma-Aldrich) in 100 mM ABC buffer (pH 7.5) and incubated for 16 h on a shaker at RT. Then, the gel pieces were washed, dehydrated and saturated with trypsin digestion buffer (12.5 ng/μL in 100 mM ABC (pH 8)) and incubated at 37 °C for 16 h on a shaker. Peptides were extracted twice with 50% acetonitrile (ACN), twice with 0.1% formic acid and once with 70% ACN and 0.1% formic acid. The supernatant from each step was pooled and vacuum dried. In the other half of the PARylation reaction mixture, cysteines were reduced (DTT, 5 mM, 56 °C, 45 min) and alkylated (IAM, 15 mM, RT, 30 min in the dark). Hydroxylamine was then added to a final concentration of 0.5 M and incubated for 16 h on a shaker at RT. Proteins were then separated by SDS-PAGE and digested with trypsin, and peptides were extracted following the same procedure described above.

Liquid chromatography-tandem mass spectrometry (LC-MS/MS) analysis

Peptides were redissolved in 10 μL of 0.4% acetic acid, and 4 μL of this solution was used for LC-MS/MS analysis. In brief, using an Eksigent NanoLC-2D system, peptides were trapped on a trap column packed in-house (1.5 cm × 75 μm, i.d.) with C18 beads (5 μm, 200 Å, Dr. Maisch GmbH). Next, peptides were eluted onto an analytical column (15 cm × 75 μm i.d.) packed in-house with C18 beads (5 μm, 120 Å, Dr. Maisch GmbH) using a linear gradient from 5% to 40% buffer B (ACN with 0.1% formic acid) over 90 min at a flow rate of 300 nL/min (total run time = 120 min). With a linear trap quadrupole (LTQ) Orbitrap XL (Thermo Scientific) mass spectrometer, full-scan survey spectra were acquired in the Orbitrap mass analyzer in the m/z range of 300–1800 at a resolution of 60,000. For ionization, the capillary temperature and spray voltage were set to 250 °C and 2.1 kV, respectively. The ten most intense ions from the MS1 scan were fragmented using collision-induced dissociation (CID) in the LTQ (normalized collision energy, 35%; dynamic exclusion, 60 s).

LC-MS/MS data analysis

The raw files were subjected to a database search using Proteome Discoverer (v. 2.2.0.388) with the default workflow against a combined database containing protein sequences from the UniProt SwissProt Human database (accessed Sep. 26, 2019) together with sequences of contaminant proteins from the common Repository of Adventitious Proteins (cRAP) and the BAP1 protein sequence (His6-BAP1 sequence, obtained from Boston Biochem, catalog number E-345). The SEQUEST HT search parameters were set as follows: enzyme (trypsin, semi), maximum allowed missed cleavages = 2, MS tolerance = 15 ppm, and MS/MS tolerance = 0.5 Da. Carbamidomethylation of cysteine (+57.021 Da) was kept as a fixed modification. Oxidation (+15.995 Da) of methionine, hydroxamic acid (+15.011 Da) modification of aspartic acid (Asp) and glutamic acid (Glu) and deamidation (+0.984 Da) of asparagine (Asn) and glutamine (Gln) were kept as variable modifications. Only high-confidence identifications were used for further analysis.

Laser microirradiation and cell imaging

Laser microirradiation assay was performed as previously described [64]. After transfection with the vectors expressing the indicated GFP-tagged proteins in four-well plates for 48 h, U2OS cells were incubated with 10 μM 5-bromo-2′-deoxyuridine for 24 h and subjected to laser microirradiation using a Nikon A1 laser microdissection system (Nikon). Ten cells per well were subjected to laser treatment for 10 s under a 60× oil objective using a fixed-wavelength UV-A laser (405 nm) in a temperature-controlled chamber with a CO_2 supplier. After laser treatment, cells were incubated at 37 °C for the indicated times. The intensity of each laser stripe at each time point was determined using a confocal microscope. Kinetic analyses were performed using NIS Elements C software (Nikon). Each data series was normalized with respect to the baseline values.

Lentivirus production

Lentiviral vectors were transfected into 293T cells using FuGENE HD transfection reagent (Promega). After 48 h, the lentivirus-containing medium was harvested and filtered through a 0.45 μm syringe filter to remove residual 293T cells. The filtered lentivirus-containing medium was used for cell infection.

Statistical analysis

All experimental data were expressed as mean ± s.d. wherever applicable. The significance of differences between measurements was evaluated by Student's *t* test using Microsoft Excel. *P* values shown on the graphs are indicated with the following asterisk code: $*p < 0.05$; $**p < 0.01$; $***p < 0.001$. A *p* value > 0.05 was considered not significant (*ns*) unless otherwise indicated.

DATA AVAILABILITY

The detailed experimental procedures and the materials used in this study will be freely available upon request. Please contact jongkwon@ewha.ac.kr.

REFERENCES

1. Marteijn JA, Lans H, Vermeulen W, Hoeijmakers JH. Understanding nucleotide excision repair and its roles in cancer and ageing. Nat Rev Mol Cell Biol. 2014;15:465–81.
2. Sugasawa K. Molecular mechanisms of DNA damage recognition for mammalian nucleotide excision repair. DNA Repair. 2016;44:110–7.
3. Ray Chaudhuri A, Nussenzweig A. The multifaceted roles of PARP1 in DNA repair and chromatin remodelling. Nat Rev Mol Cell Biol. 2017;18:610–21.
4. Kraus WL. PARPs and ADP-Ribosylation: 50 Years … and Counting. Mol Cell. 2015;58:902–10.
5. Cohen MS, Chang P. Insights into the biogenesis, function, and regulation of ADP-ribosylation. Nat Chem Biol. 2018;14:236–43.

6. Gupte R, Liu Z, Kraus WL. PARPs and ADP-ribosylation: recent advances linking molecular functions to biological outcomes. Genes & development. 2017;31:101–26.
7. Alemasova EE, Lavrik OI. Poly(ADP-ribosyl)ation by PARP1: reaction mechanism and regulatory proteins. Nucleic Acids Res. 2019;47:3811–27.
8. Robu M, Shah RG, Purohit NK, Zhou P, Naegeli H, Shah GM. Poly(ADP-ribose) polymerase 1 escorts XPC to UV-induced DNA lesions during nucleotide excision repair. Proc Natl Acad Sci USA. 2017;114:E6847–E6856.
9. Robu M, Shah RG, Petitclerc N, Brind'Amour J, Kandan-Kulangara F, Shah GM. Role of poly(ADP-ribose) polymerase-1 in the removal of UV-induced DNA lesions by nucleotide excision repair. Proc Natl Acad Sci USA. 2013;110:1658–63.
10. Pines A, Vrouwe MG, Marteijn JA, Typas D, Luijsterburg MS, Cansoy M, et al. PARP1 promotes nucleotide excision repair through DDB2 stabilization and recruitment of ALC1. J Cell Biol. 2012;199:235–49.
11. King BS, Cooper KL, Liu KJ, Hudson LG. Poly(ADP-ribose) contributes to an association between poly(ADP-ribose) polymerase-1 and xeroderma pigmentosum complementation group A in nucleotide excision repair. J Biol Chem. 2012;287:39824–33.
12. Jensen DE, Proctor M, Marquis ST, Gardner HP, Ha SI, Chodosh LA, et al. BAP1: a novel ubiquitin hydrolase which binds to the BRCA1 RING finger and enhances BRCA1-mediated cell growth suppression. Oncogene. 1998;16:1097–112.
13. Carbone M, Yang H, Pass HI, Krausz T, Testa JR, Gaudino G. BAP1 and cancer. Nat Rev Cancer. 2013;13:153–9.
14. Masclef L, Ahmed O, Estavoyer B, Larrivee B, Labrecque N, Nijnik A, et al. Roles and mechanisms of BAP1 deubiquitinase in tumor suppression. Cell Death Differ. 2021;28:606–25.
15. Szczepanski AP, Wang L. Emerging multifaceted roles of BAP1 complexes in biological processes. Cell Death Disco. 2021;7:20.
16. Abdel-Rahman MH, Pilarski R, Cebulla CM, Massengill JB, Christopher BN, Boru G, et al. Germline BAP1 mutation predisposes to uveal melanoma, lung adenocarcinoma, meningioma, and other cancers. J Med Genet. 2011;48:856–9.
17. Bott M, Brevet M, Taylor BS, Shimizu S, Ito T, Wang L, et al. The nuclear deubiquitinase BAP1 is commonly inactivated by somatic mutations and 3p21.1 losses in malignant pleural mesothelioma. Nat Genet. 2011;43:668–72.
18. Guo G, Gui Y, Gao S, Tang A, Hu X, Huang Y, et al. Frequent mutations of genes encoding ubiquitin-mediated proteolysis pathway components in clear cell renal cell carcinoma. Nat Genet. 2012;44:17–19.
19. Harbour JW, Onken MD, Roberson ED, Duan S, Cao L, Worley LA, et al. Frequent mutation of BAP1 in metastasizing uveal melanomas. Science. 2010;330:1410–3.
20. Pena-Llopis S, Vega-Rubin-de-Celis S, Liao A, Leng N, Pavia-Jimenez A, Wang S, et al. BAP1 loss defines a new class of renal cell carcinoma. Nat Genet. 2012;44:751–9.
21. Testa JR, Cheung M, Pei J, Below JE, Tan Y, Sementino E, et al. Germline BAP1 mutations predispose to malignant mesothelioma. Nat Genet. 2011;43:1022–5.
22. Carbone M, Adusumilli PS, Alexander HR Jr, Baas P, Bardelli F, Bononi A, et al. Mesothelioma: Scientific clues for prevention, diagnosis, and therapy. CA Cancer J Clin. 2019;69:402–29.
23. Napolitano A, Pellegrini L, Dey A, Larson D, Tanji M, Flores EG, et al. Minimal asbestos exposure in germline BAP1 heterozygous mice is associated with deregulated inflammatory response and increased risk of mesothelioma. Oncogene. 2016;35:1996–2002.
24. Kadariya Y, Cheung M, Xu J, Pei J, Sementino E, Menges CW, et al. Bap1 Is a Bona Fide Tumor Suppressor: Genetic Evidence from Mouse Models Carrying Heterozygous Germline Bap1 Mutations. Cancer Res. 2016;76:2836–44.
25. Xu J, Kadariya Y, Cheung M, Pei J, Talarchek J, Sementino E, et al. Germline mutation of Bap1 accelerates development of asbestos-induced malignant mesothelioma. Cancer Res. 2014;74:4388–97.
26. Dey A, Seshasayee D, Noubade R, French DM, Liu J, Chaurushiya MS, et al. Loss of the tumor suppressor BAP1 causes myeloid transformation. Science. 2012;337:1541–6.
27. Machida YJ, Machida Y, Vashisht AA, Wohlschlegel JA, Dutta A. The deubiquitinating enzyme BAP1 regulates cell growth via interaction with HCF-1. J Biol Chem. 2009;284:34179–88.
28. Misaghi S, Ottosen S, Izrael-Tomasevic A, Arnott D, Lamkanfi M, Lee J, et al. Association of C-terminal ubiquitin hydrolase BRCA1-associated protein 1 with cell cycle regulator host cell factor 1. Mol Cell Biol. 2009;29:2181–92.
29. Eletr ZM, Wilkinson KD. An emerging model for BAP1's role in regulating cell cycle progression. Cell Biochem Biophys. 2011;60:3–11.
30. Affar EB, Carbone M. BAP1 regulates different mechanisms of cell death. Cell Death Dis. 2018;9:1151.
31. Yu H, Pak H, Hammond-Martel I, Ghram M, Rodrigue A, Daou S, et al. Tumor suppressor and deubiquitinase BAP1 promotes DNA double-strand break repair. Proc Natl Acad Sci USA. 2014;111:285–90.
32. Eletr ZM, Yin L, Wilkinson KD. BAP1 is phosphorylated at serine 592 in S-phase following DNA damage. FEBS Lett. 2013;587:3906–11.
33. Klusmann I, Wohlberedt K, Magerhans A, Teloni F, Korbel JO, Altmeyer M, et al. Chromatin modifiers Mdm2 and RNF2 prevent RNA:DNA hybrids that impair DNA replication. Proc Natl Acad Sci USA. 2018;115:E11311–E11320.
34. Lee HS, Lee SA, Hur SK, Seo JW, Kwon J. Stabilization and targeting of INO80 to replication forks by BAP1 during normal DNA synthesis. Nat Commun. 2014;5:5128.
35. Lee HS, Seo HR, Lee SA, Choi S, Kang D, Kwon J. BAP1 promotes stalled fork restart and cell survival via INO80 in response to replication stress. Biochemical J. 2019;476:3053–66.
36. Peng J, Ma J, Li W, Mo R, Zhang P, Gao K, et al. Stabilization of MCRS1 by BAP1 prevents chromosome instability in renal cell carcinoma. Cancer Lett. 2015;369:167–74.
37. Ismail IH, Davidson R, Gagne JP, Xu ZZ, Poirier G, Hendzel MJ Germ-line Mutations in BAP1 Impair its Function in DNA Double-Strand break Repair. Cancer Res. 2014.
38. Muster B, Rapp A, Cardoso MC. Systematic analysis of DNA damage induction and DNA repair pathway activation by continuous wave visible light laser microirradiation. AIMS Genet. 2017;4:47–68.
39. Wakasugi M, Sasaki T, Matsumoto M, Nagaoka M, Inoue K, Inobe M, et al. Nucleotide excision repair-dependent DNA double-strand break formation and ATM signaling activation in mammalian quiescent cells. J Biol Chem. 2014;289:28730–7.
40. Ray A, Milum K, Battu A, Wani G, Wani AA. NER initiation factors, DDB2 and XPC, regulate UV radiation response by recruiting ATR and ATM kinases to DNA damage sites. DNA Repair. 2013;12:273–83.
41. Zhang Y, Wang J, Ding M, Yu Y. Site-specific characterization of the Asp- and Glu-ADP-ribosylated proteome. Nat Methods. 2013;10:981–4.
42. Gibson BA, Kraus WL. New insights into the molecular and cellular functions of poly(ADP-ribose) and PARPs. Nat Rev Mol Cell Biol. 2012;13:411–24.
43. Bergink S, Salomons FA, Hoogstraten D, Groothuis TA, de Waard H, Wu J, et al. DNA damage triggers nucleotide excision repair-dependent monoubiquitylation of histone H2A. Genes Dev. 2006;20:1343–52.
44. Kapetanaki MG, Guerrero-Santoro J, Bisi DC, Hsieh CL, Rapic-Otrin V, Levine AS. The DDB1-CUL4ADDB2 ubiquitin ligase is deficient in xeroderma pigmentosum group E and targets histone H2A at UV-damaged DNA sites. Proc Natl Acad Sci USA. 2006;103:2588–93.
45. Zhu Q, Wani G, Arab HH, El-Mahdy MA, Ray A, Wani AA. Chromatin restoration following nucleotide excision repair involves the incorporation of ubiquitinated H2A at damaged genomic sites. DNA Repair. 2009;8:262–73.
46. Chitale S, Richly HDICER. and ZRF1 contribute to chromatin decondensation during nucleotide excision repair. Nucleic Acids Res. 2017;45:5901–12.
47. Marteijn JA, Bekker-Jensen S, Mailand N, Lans H, Schwertman P, Gourdin AM, et al. Nucleotide excision repair-induced H2A ubiquitination is dependent on MDC1 and RNF8 and reveals a universal DNA damage response. Cell Biol. 2009;186:835–47.
48. Sarkar S, Kiely R, McHugh PJ. The Ino80 chromatin-remodeling complex restores chromatin structure during UV DNA damage repair. J Cell Biol. 2010;191:1061–8.
49. Jiang Y, Wang X, Bao S, Guo R, Johnson DG, Shen X, et al. INO80 chromatin remodeling complex promotes the removal of UV lesions by the nucleotide excision repair pathway. Proc Natl Acad Sci USA. 2010;107:17274–9.
50. Rathkey D, Khanal M, Murai J, Zhang J, Sengupta M, Jiang Q, et al. Sensitivity of Mesothelioma Cells to PARP Inhibitors Is Not Dependent on BAP1 but Is Enhanced by Temozolomide in Cells With High-Schlafen 11 and Low-O6-methylguanine-DNA Methyltransferase Expression. J Thorac Oncol. 2020;15:843–59.
51. Carbone M, Pass HI, Ak G, Alexander HR Jr, Baas P, Baumann F, et al. Medical and surgical care of mesothelioma patients and their relatives carrying germline BAP1 mutations. J Thorac Oncol. 2022;S1556-0864:00192–7.
52. Ghafoor A, Mian I, Wagner C, Mallory Y, Agra MG, Morrow B, et al. Phase 2 Study of Olaparib in Malignant Mesothelioma and Correlation of Efficacy With Germline or Somatic Mutations in BAP1. Gene. JTO Clin Res Rep. 2021;2:100231.
53. Bononi A, Giorgi C, Patergnani S, Larson D, Verbruggen K, Tanji M, et al. BAP1 regulates IP3R3-mediated Ca(2+) flux to mitochondria suppressing cell transformation. Nature. 2017;546:549–53.
54. Sime W, Niu Q, Abassi Y, Masoumi KC, Zarrizi R, Kohler JB, et al. BAP1 induces cell death via interaction with 14-3-3 in neuroblastoma. Cell Death Dis. 2018;9:458.
55. He M, Chaurushiya MS, Webster JD, Kummerfeld S, Reja R, Chaudhuri S, et al. Intrinsic apoptosis shapes the tumor spectrum linked to inactivation of the deubiquitinase BAP1. Science. 2019;364:283–5.
56. Zhang Y, Shi J, Liu X, Feng L, Gong Z, Koppula P, et al. BAP1 links metabolic regulation of ferroptosis to tumour suppression. Nat Cell Biol. 2018;20:1181–92.
57. Lee JW, Kim JE, Park EJ, Kim JH, Lee CH, Lee SR, et al. Two conserved cysteine residues are critical for the enzymic function of the human platelet-derived growth factor receptor-beta: evidence for different roles of Cys-822 and Cys-940 in the kinase activity. Biochem J. 2004;382:631–9.

58. Lee D, Lee DY, Hwang YS, Seo HR, Lee SA, Kwon J. The Bromodomain Inhibitor PFI-3 Sensitizes Cancer Cells to DNA Damage by Targeting SWI/SNF. Mol Cancer Res: MCR. 2021;19:900–12.
59. Robu M, Shah RG, Shah GM. Methods to Study Intracellular Movement and Localization of the Nucleotide Excision Repair Proteins at the DNA Lesions in Mammalian Cells. Front Cell Dev Biol. 2020;8:590242.
60. Park SG, Lee D, Seo HR, Lee SA, Kwon J. Cytotoxic activity of bromodomain inhibitor NVS-CECR2-1 on human cancer cells. Sci Rep. 2020;10:16330.
61. Sahtoe DD, van Dijk WJ, Ekkebus R, Ovaa H, Sixma TK. BAP1/ASXL1 recruitment and activation for H2A deubiquitination. Nat Commun. 2016;7:10292.
62. Mashtalir N, Daou S, Barbour H, Sen NN, Gagnon J, Hammond-Martel I, et al. Autodeubiquitination protects the tumor suppressor BAP1 from cytoplasmic sequestration mediated by the atypical ubiquitin ligase UBE2O. Mol Cell. 2014;54:392–406.
63. Seo HR, Jeong D, Lee S, Lee HS, Lee SA, Kang SW, et al. CHIP and BAP1 Act in Concert to Regulate INO80 Ubiquitination and Stability for DNA Replication. Molecules Cells. 2021;44:101–15.
64. Soo Lee N, Jin Chung H, Kim HJ, Yun Lee S, Ji JH, Seo Y, et al. TRAIP/RNF206 is required for recruitment of RAP80 to sites of DNA damage. Nat Commun. 2016;7:10463.

ACKNOWLEDGEMENTS

We thank Mi Young Kim and William Kraus for providing the pQCXIH-PARP1-His_6/FLAG vector. Funding: This work was supported by grants 2021R1A2C1008613, 2019R1A5A6099645 and 2017M3A9F9030559 from the National Research Foundation of Korea.

AUTHOR CONTRIBUTIONS

SAL initiated the study and generated most of the key initial data. DL produced the data for the repair activity of BAP1 and the related functions of PARP1. MK generated the data for the PARP1 effects on BAP1 activity, and SK for the in vivo BAP1 PARylation and the functional analysis of the BAP1 PARylation sites. SJK was responsible for the identification of PARP1 as a BAP1 binding partner. HRS obtained the results for the PARPi effects on BAP1 stability. PK and CL identified the BAP1 PARylation sites by LC-MS/MS. NSL and HK generated the laser microirradiation data. HSL provided important technical assistance and data interpretation. All authors contributed to data analysis and interpretation, and manuscript preparation. SAL and JK wrote the manuscript. JK conceived and supervised the entire project.

FUNDING

This work was supported by grants 2021R1A2C1008613, 2019R1A5A6099645 and 2017M3A9F9030559 from the National Research Foundation of Korea.

COMPETING INTERESTS

The authors declare no competing interests.

ADDITIONAL INFORMATION

Supplementary information The online version contains supplementary material available at https://doi.org/10.1038/s41418-022-01024-w.

Correspondence and requests for materials should be addressed to Jongbum Kwon.

Reprints and permission information is available at http://www.nature.com/reprints

Publisher's note Springer Nature remains neutral with regard to jurisdictional claims in published maps and institutional affiliations.